The miR-200–Zeb1 axis regulates key aspects of β-cell function and survival in vivo

Original Article

MOLECULAR METABOLISM

The miR-200—Zeb1 axis regulates key aspects of β-cell function and survival *in vivo*

Alexandra C. Title [1,2], Pamuditha N. Silva [1], Svenja Godbersen [1], Lynn Hasenöhrl [1], Markus Stoffel [1,2,3,*]

ABSTRACT

Objective: The miR-200—Zeb1 axis regulates the epithelial-to-mesenchymal transition (EMT), differentiation, and resistance to apoptosis. A better understanding of these processes in diabetes is highly relevant, as β-cell dedifferentiation and apoptosis contribute to the loss of functional β-cell mass and diabetes progression. Furthermore, EMT promotes the loss of β-cell identity in the *in vitro* expansion of human islets. Though the miR-200 family has previously been identified as a regulator of β-cell apoptosis *in vivo*, studies focusing on Zeb1 are lacking. The aim of this study was thus to investigate the role of Zeb1 in β-cell function and survival *in vivo.*

Methods: miR-200 and Zeb1 are involved in a double-negative feedback loop. We characterized a mouse model in which miR-200 binding sites in the *Zeb1* 3′UTR are mutated (*Zeb1*^{200}), leading to a physiologically relevant upregulation of *Zeb1* mRNA expression. The role of Zeb1 was investigated in this model via metabolic tests and analysis of isolated islets. Further insights into the distinct contributions of the miR-200 and Zeb1 branches of the feedback loop were obtained by crossing the *Zeb1*^{200} allele into a background of miR-141—200c overexpression.

Results: Mild *Zeb1* derepression *in vivo* led to broad transcriptional changes in islets affecting β-cell identity, EMT, insulin secretion, cell—cell junctions, the unfolded protein response (UPR), and the response to ER stress. The aggregation and insulin secretion of dissociated islets of mice homozygous for the *Zeb1*^{200} mutation (*Zeb1*^{200M}) were impaired, and *Zeb1*^{200M} islets were resistant to thapsigargin-induced ER stress *ex vivo*. *Zeb1*^{200M} mice had increased circulating proinsulin levels but no overt metabolic phenotype, reflecting the strong compensatory ability of islets to maintain glucose homeostasis.

Conclusions: This study signifies the importance of the miR-200—Zeb1 axis in regulating key aspects of β-cell function and survival. A better understanding of this axis is highly relevant in developing therapeutic strategies for inducing β-cell redifferentiation and maintaining β-cell identity in *in vitro* islet expansion.

Keywords β-cell dedifferentiation; Epithelial-to-mesenchymal transition; Double-negative feedback loop; Islet aggregation; ER stress; microRNA

1. INTRODUCTION

The global prevalence of diabetes was estimated to be 9.3% of the adult population, or 463 million people, in 2019, with projections for a 25% increase by 2030 [1]. Glucose homeostasis is dependent on the proper functioning and survival of pancreatic β-cells. Type 2 diabetes (T2D) pathophysiology is centered around a chronic and increased demand on pancreatic β-cells for sufficient insulin secretion, which surpasses their compensatory ability and ultimately leads to β-cell exhaustion and apoptosis [2,3]. In recent years, there has been a growing understanding that the loss of functional β-cell mass may not simply depend on apoptosis but also the loss of β-cell function and impaired insulin secretion via dedifferentiation [4,5]. In parallel, islets from T2D patients express increased levels of the mesenchymal marker vimentin, indicating that an epithelial-to-mesenchymal transition (EMT) may further contribute to a loss of β-cell identity and diabetes progression [6—8]. EMT also occurs in *in vitro* monolayer cultures of human islets [9—12], which is not only relevant for the field of islet transplantation, as *in vitro* expansion could help increase the supply of human β-cells, but also points to the importance of epithelial junctions and cell—cell contacts in β-cell function [12]. Therefore, advancing our knowledge on the molecular mechanisms controlling β-cell identity, function, and survival is essential to understanding β-cell demise in diabetes and developing potential therapeutic interventions. In mammals, microRNAs (miRNA) are ~22-nucleotide-long noncoding RNAs that most often repress the expression of target mRNAs post-transcriptionally through the specific binding to seed regions in their 3' UTR [13]. A given miRNA generally has hundreds of target mRNAs, and thus, usually acts by modulating the expression of many target genes, which can cumulatively lead to major phenotypic consequences [14]. The miR-200 family (referred to as miR-200 for simplicity) comprises five miRNAs divided into two genomic clusters: *Mir-*

[1]Institute of Molecular Health Sciences (IMHS), ETH Zürich, Otto-Stern-Weg 7, 8093, Zürich, Switzerland [2]Competence Center Personalized Medicine, ETH Zürich, Voltastrasse 24, 8044, Zürich, Switzerland [3]Medical Faculty, University of Zürich, 8091, Zürich, Switzerland

*Corresponding author. Institute of Molecular Health Sciences (IMHS), ETH Zürich, Otto-Stern-Weg 7, 8093, Zürich, Switzerland. E-mail: stoffel@biol.ethz.ch (M. Stoffel).

Abbreviations: EMT, epithelial-to-mesenchymal transition; EMT TF, EMT transcription factor; T2D, type 2 diabetes; T1D, type 1 diabetes; miRNA, microRNA; UPR, unfolded protein response; MET, mesenchymal-to-epithelial transition; Tg, thapsigargin; GSIS, glucose-stimulated insulin secretion; iPSC, induced pluripotent stem cells

Received March 31, 2021 • Revision received May 24, 2021 • Accepted June 3, 2021 • Available online 8 June 2021

https://doi.org/10.1016/j.molmet.2021.101267

200b~200~429 and *Mir-200c~141*. These miRNAs can also be subdivided into two functional families based on their seed region: miR-200b, miR-200c, and miR-429 share one seed (AAUACUG), and miR-200a and miR-141 share a seed that differs by a single base (AACACUG) [15]. miR-200 is highly expressed in islets and has been previously identified as a regulator of apoptosis and differentiation in β-cells [16–18]. It has also been extensively studied in the context of cancer as a regulator of EMT [19], mostly via its repression of the EMT transcription factor (EMT-TF), Zeb1 [15,20,21]. Interestingly, the modulation of EMT, mediated by miR-200 and Zeb1, is accentuated by the reinforcing activity of a double-negative feedback loop that exists between these two factors [22–24].

Zeb1 is best studied as an EMT-TF that drives tumor invasion and metastasis [21,25]. In addition, Zeb1 also plays critical roles in wound healing and embryonic development [26–28]. Zeb1 has only been studied in a limited manner in islets, namely as a contributor to EMT and the dedifferentiation of human islets in culture [11]; its function in β-cells *in vivo* has not been investigated. *Zeb1* is a unique and intriguing miR-200 target gene, as its 3' UTR harbors nine conserved binding sites for miR-200 in mice and eight in humans [29,30]. Fewer than 2% of miRNA target genes have more than two binding sites for a particular miRNA [31], and as the site number is correlated with the repressive activity of miRNAs [13,32], *Zeb1* is predicted to be a particularly robust miR-200 target gene and potentially a major contributor to miR-200-mediated phenotypes. This was recently observed *in vivo* in an insulinoma mouse model, in which dissociation of *Zeb1* mRNA from miR-200 repression phenocopied miR-200-ablation in mediating a phenotype of tumor dedifferentiation and invasion [25].

Thus, the miR-200 family and Zeb1 have been previously described as regulators of differentiation, EMT, and survival, all of which are important modulators of functional β-cell mass in diabetes pathophysiology. Though the function of miR-200 in β-cells has been studied *in vivo* [16], that of Zeb1 has not been addressed. To identify the role of Zeb1 in β-cells, we utilized a previously generated mouse model in which miR-200 binding sites in the *Zeb1* 3′UTR are genetically mutated (*Zeb1*^{200}), leading to a mild and physiologically relevant upregulation of *Zeb1* mRNA expression [25]. By crossing the *Zeb1*^{200} allele into a mouse model with β-cell-specific overexpression of miR-141–200c (*RipmiR-141~200c*), we further sought to disentangle the miR-200 and Zeb1 branches of the double-negative feedback loop. Using these models, we describe the functions of Zeb1 in regulating critical aspects of β-cell biology, including islet aggregation, β-cell identity, insulin secretion, and resistance to apoptosis and ER stress through the combinatorial regulation of both direct ZEB1 target genes and miR-200 target genes via the miR-200–Zeb1 double-negative feedback loop.

2. MATERIALS AND METHODS

2.1. Experimental animals

Mice were housed in a pathogen-free animal facility at the Institute of Molecular Health Sciences in ETH Zürich, in a temperature-controlled room (22 °C) with humidity at 55%, and on a 12 h light–dark cycle (lights on from 6:00 to 18:00). Mice were fed standard laboratory chow and water *ad libitum*. All ethical regulations were followed, and all animal experiments were approved by the Kantonale Veterinäramt Zürich. The generation of mice with mutated miR-200 binding sites in the *Zeb1* 3′UTR (*Zeb1*^{200}) was described previously [25], along with the generation of mice with β-cell-specific overexpression of miR-141–200c (*RipmiR-141~200c*) [16].

2.2. Fasted plasma samples

Mice were fasted for 6 h and blood-sampled from the tail into EDTA-containing tubes. Samples were centrifuged for plasma separation (8 min, 10,000×*g*, 4 °C). Plasma insulin was measured using the Rat Ultrasensitive Insulin ELISA kit (Alpco), and plasma proinsulin was measured using the Rat/Mouse Proinsulin ELISA kit (Mercodia).

2.3. Longitudinal measurements and *in vivo* metabolic testing

All blood glucose measurements were made using a Contour XT glucometer (Bayer). For longitudinal monitoring, body weight and random-fed blood glucose were measured weekly at the same time of day (mid-afternoon). For metabolic tests, mice were fasted for 6 h before intraperitoneal injection with 2.5 g/kg glucose (IPGTT), 0.9 U/kg insulin (IPITT), or 2 g/kg pyruvate (IPPTT). Blood glucose was measured immediately before injection and at 15, 30, 45, 60, 90, and 120 min post-injection. For *in vivo* insulin secretion tests, mice were fasted for 6 h and blood-sampled before intraperitoneal injection with 2.5 g/kg glucose. Blood was further sampled at 15 and 30 min. Plasma insulin was measured using the Rat Ultrasensitive Insulin ELISA kit (Alpco).

2.4. Primary islet isolation and culture

Islet isolation was performed as previously described [33] with slight modifications. In brief, 5 mg/mL Liberase TM (Roche) was diluted in RPMI buffer (Invitrogen) to a concentration of 0.2 mg/mL and perfused via the common bile duct into the pancreas, which was then removed and incubated for 17 min at 37 °C. Islets were separated from exocrine cells by centrifugation with Histopaque 1077 (Sigma) and further purified using a 70 μm filter (Miltenyi). Islets were handpicked and cultured in RPMI 1640 containing 11.1 mM glucose and supplemented with 10% FBS, 100 U/mL penicillin, and 100 μg/mL streptomycin.

2.5. Islet reaggregation

Isolated islets were dispersed with 0.25% trypsin and seeded into GravityPLUS plates (InSphero) at a density of 2000 cells per hanging drop. Aggregation was allowed to occur for 4 days, at which point reaggregated islets were dropped into recipient low-attachment wells. Insulin secretion assays and imaging were performed on the same day or 1 day after reaggregated islets were dropped. For adenovirus-treated reaggregated islets, dispersed islets were reaggregated in the presence of adenovirus particles mixed into the media used for hanging drop formation (MOI 200).

2.6. Reaggregated islet morphology characterization

Reaggregated islet morphology was analyzed on ImageJ. A variance filter and the ImageJ auto-threshold were used to generate an outline of the islet. Circularity was defined as 4π*area/perimeterˆ2 of this shape, where 1 represents a perfect circle, and increased tortuosity decreases circularity.

2.7. Insulin secretion assays

For insulin secretion assays from native islets, islets were isolated from mice and allowed to recover overnight. Islets were handpicked and size-matched in pools of ~25–30 islets. Islets were starved in KRBH buffer in the absence of glucose for 2 h, then incubated with 3.3 mM glucose KRBH buffer for basal insulin secretion measurements, followed by a 1-hour incubation with secretagogues in KRBH buffer (high glucose, KCl, GLP-1). Supernatants were collected after each incubation and centrifuged to remove any remaining cells. At the end of the experiment, islets were acid-ethanol extracted (15 mM HCl, 75% EtOH, 0.1% Triton-X) for total insulin content measurements. For insulin secretion assays from reaggregated islets, a similar process was

followed, except assays were performed from single reaggregated islets in 20 μL hanging drops of KRBH buffer. Insulin measurements were performed from appropriately diluted samples using the Rat Ultrasensitive Insulin ELISA kit (Alpco).

2.8. Cell culture experiments

INS-1E cells were cultured in RPMI 1640 media (Thermo Fisher) supplemented with 11.1 mM glucose, 10% FBS, 10 mM HEPES, 1 mM Pyruvate, 50 μM beta-mercaptoethanol, 2 mM Glutamax, and P/S (100 U/mL penicillin and 100 μg/mL streptomycin). For siRNA-knockdown experiments, cells were reverse-transfected with 20 nM scramble siRNA or Zeb1 siRNA (Dharmacon, ONTARGETplus SMARTpool) using RNAiMax (Thermo Fisher). siRNA sequences are listed in Supplemental Table 1. For adenovirus treatment, INS-1E-containing wells seeded the previous day were treated with Ad-GFP (control) or Ad-Zeb1 (MOI 5), and the medium was exchanged 8 h after transduction.

2.9. Thapsigargin ER stress experiments

Islets were isolated and allowed to recover overnight. Islets were then pooled according to genotype and separated into replicate wells. Control islets were cultured in standard islet media, and treatment islets were cultured for 48 h in a high-glucose islet media (25 mM glucose), followed by 6 or 20 h of treatment with 1 μM thapsigargin (Sigma). Samples were harvested, washed with PBS, and used either for RNA or protein extraction. For INS-1E experiments, cells were treated with 500 nM thapsigargin for 6 h, 60 h after siRNA transfection or 48 h after adenovirus treatment.

2.10. Immunofluorescence staining

Pancreata were fixed in 4% paraformaldehyde, embedded in paraffin, and cut into 3.5 μm sections. Antigen retrieval was performed with a 10 mM sodium citrate buffer (pH 6.0). Sections were permeabilized and blocked in phosphate buffered saline (PBS) containing 0.1% Triton-X-100, 1% bovine serum albumin (BSA), and 5% donkey or goat serum. Primary antibody binding was performed overnight at 4 °C, whereas secondary antibody incubation was performed at room temperature for 1 h. Slides were scanned using a 20× objective on the Pannoramic 250 Slide scanner (3D Histech). TdT-mediated dUTP-biotin nick end labeling (TUNEL) staining was performed using the Click-iT TUNEL Alexa Fluor Imaging Assay (Invitrogen) with the following modification: after deparaffinization, slides were incubated with Proteinase K for 15 min, rinsed, and immersed in 4% paraformaldehyde for 5 min before continuing with the protocol. Antibodies used for immunofluorescence staining are listed in Supplemental Table 2.

2.11. Image analysis

For the determination of β-cell mass, four pancreatic sections spread 500 μm apart were stained with anti-insulin antibody per mouse. Slidescanner images were exported in a Pannoramic Viewer (3D Histech) and analyzed using Qupath [34]. Pancreatic β-cell mass was calculated as the ratio of the number of β-cells/total number of DAPI nuclei x pancreas wet weight. For TUNEL analysis, two sections per mouse were co-stained with the TUNEL assay and anti-insulin antibody. Images were analyzed in ImageJ, and data were calculated as % TUNEL positive nuclei of the total number of β-cells per section.

2.12. Confocal imaging analysis

Immunofluorescence staining was performed to label UCN3 and Insulin with Cy5 and Alexa 488 fluorophores. Each fluorophore was imaged sequentially on a Leica SP8 confocal microscope using 633 nm and 488 nm laser lines, and emission was collected with HyD detectors with bandpass filters set to 508—631 nm and 664—784 nm, respectively. Analysis was performed on ImageJ, where islet areas were first manually outlined before a Percentile threshold on the Alexa 488 channel was applied to calculate the insulin signal intensity. The same mask was applied in the Cy5 channel to calculate the UCN3 signal intensity. Similarly, MAFA was labeled with Alexa 633 in the absence of insulin staining but using the same imaging parameters as Cy5. The Hoechst nuclear signal was used as a mask applied to the Alexa 633 channel to determine the MAFA signal intensity per islet.

2.13. miRNA and gene-expression analysis

RNA was extracted using TRI Reagent (Sigma—Aldrich). miRNA expression analysis was performed using miRNA-specific TaqMan MicroRNA Assays (Thermo Fisher). RNA was reverse transcribed using the TaqMan MicroRNA Reverse Transcription Kit (Thermo Fisher), and qPCR was performed with the TaqMan Universal PCR Master Mix No Amp UNG (Thermo Fisher). For gene-expression analysis, RNA was reverse transcribed using the High-Capacity cDNA Reverse Transcription kit (Thermo Fisher), and qPCR was conducted using gene-specific primers and 2x KAPA SYBR FAST qPCR MM (Kapa Biosystems). Relative expression values were calculated using the ddCT and standard curve methods, employing snoRNA202 for miRNA or mouse *36b4* (*Rplp0*) for gene-expression normalization in mouse samples, and miR-16 for miRNA or rat *36b4* (*Rplp0*) for gene-expression normalization in rat samples. TaqMan assays and qPCR primers used are listed in Supplemental Table 1.

2.14. Immunoblotting

Samples were disrupted in RIPA buffer (150 nM NaCl, 1% Triton-X, 50 mM Tris, 0.5% sodium deoxycholate, 0.1% SDS), supplemented with Complete, EDTA-free Protease inhibitors (Roche) and Halt Phosphatase inhibitors (Pierce), and sonicated. Protein concentrations were measured by bicinchoninic acid assay (BCA). Laemmli buffer was added to samples, and equal protein amounts were separated by sodium dodecyl sulfate—polyacrylamide gel electrophoresis (SDS-PAGE). Samples were transferred by electro-blotting to nitrocellulose membranes (Protran), and membranes were blocked in 5% milk or 5% BSA in Tris-buffered saline with Tween-20 (TBS-T) for 1 h. Membranes were incubated with appropriate antibodies overnight at 4 °C, then exposed to secondary antibodies for 1 h at room temperature and developed using ECL Western Blotting Substrate. Band density was evaluated using ImageJ. Antibodies used for immunoblotting are listed in Supplemental Table 2. The following proteins were probed together on the same blot: ZEB1 (Figure 1C), CDH1 (Figure 2F), MAFA (Figure 2B), and control HSP90 (Figures 1C, 2B, 2F); UCN3, PCSK1, and control TUBULIN (Figure 2B); p-PERK, PERK, p-IRE1α, IRE1α, GRP94, BiP, CHOP, and control BETA ACTIN (on 2 replicate blots) (Figure 5B); and pEIF2α, EIF2α, ATF6, and control BETA ACTIN (Figure 5B).

2.15. Adenoviral vectors

Recombinant adenoviruses were based on the human adenovirus type 5 (dE1/E3) backbone. Recombinant adenovirus-expressing *pre-miR-141~200c* (Ad-141—200c) was previously described [16]. In brief, 450 bp- and 250 bp-spanning sequences of *pre-miR-141~200c* were cloned into pcDNA3 and pAd5 for adenovirus production (Viraquest). Human Zeb1 adenovirus was purchased from Vectorbiolabs. Control adenovirus (Ad-Ctrl) includes GFP but lacks a transgene.

2.16. RNA sequencing

For $Zeb1^{200M}$ vs. WT mice, RNA was extracted from islets isolated from 13-to-15-week-old mice using the Picopure RNA Isolation kit

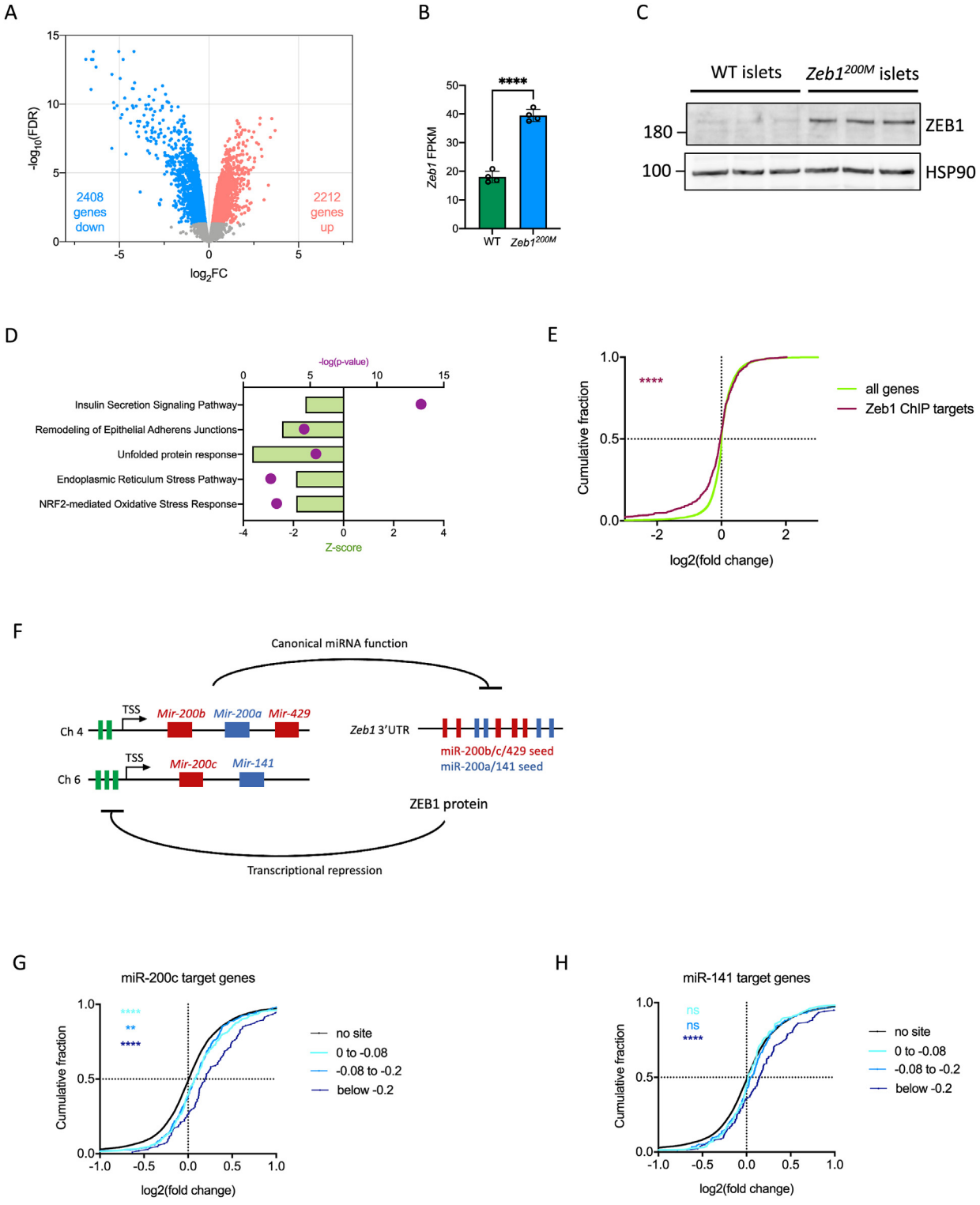

Figure 1: Mutation of miR-200-binding sites in *Zeb1* leads to regulation of the miR-200–Zeb1 feedback loop and strong transcriptional changes in unstressed islets. **(A)** Volcano plot depicting log_2FC and $-log_{10}(FDR)$ of all expressed genes in *Zeb1*^{200M} vs. WT islets. **(B)** Expression of *Zeb1* (FPKM) in WT and *Zeb1*^{200M} islets. **(C)** Immunoblotting of ZEB1 and loading control HSP90 in WT and *Zeb1*^{200M} islets (n = 1–2 mice per well). **(D)** Selected canonical pathways derived from Ingenuity analysis of significantly regulated genes in *Zeb1*^{200M} vs. WT islets. **(E)** Cumulative distribution of log_2FC of putative *Zeb1* targets in *Zeb1*^{200M} vs. WT islets. **(F)** Diagram depicting double-negative feedback loop between miR-200 family and Zeb1. **(G, H)** Cumulative distributions of log_2FC of **(G)** miR-200c and **(H)** miR-141 predicted targets subdivided by context + score in *Zeb1*^{200M} vs. WT islets. **Data information: (A–B, D–E, G–H)** RNA sequencing of *Zeb1*^{200M} vs. WT islets, n = 4, 13–15 weeks of age. **(B)** Data are plotted as mean ± SD. Significance was evaluated by two-tailed t-test **(B)**, Kolmogorov–Smirnov test **(E)**, and Kruskal–Wallis test followed by Dunn's multiple comparisons test **(G–H)**. ns, $P > 0.05$; *$P \leq 0.05$; **$P \leq 0.01$; ***$P \leq 0.001$; ****$P \leq 0.0001$.

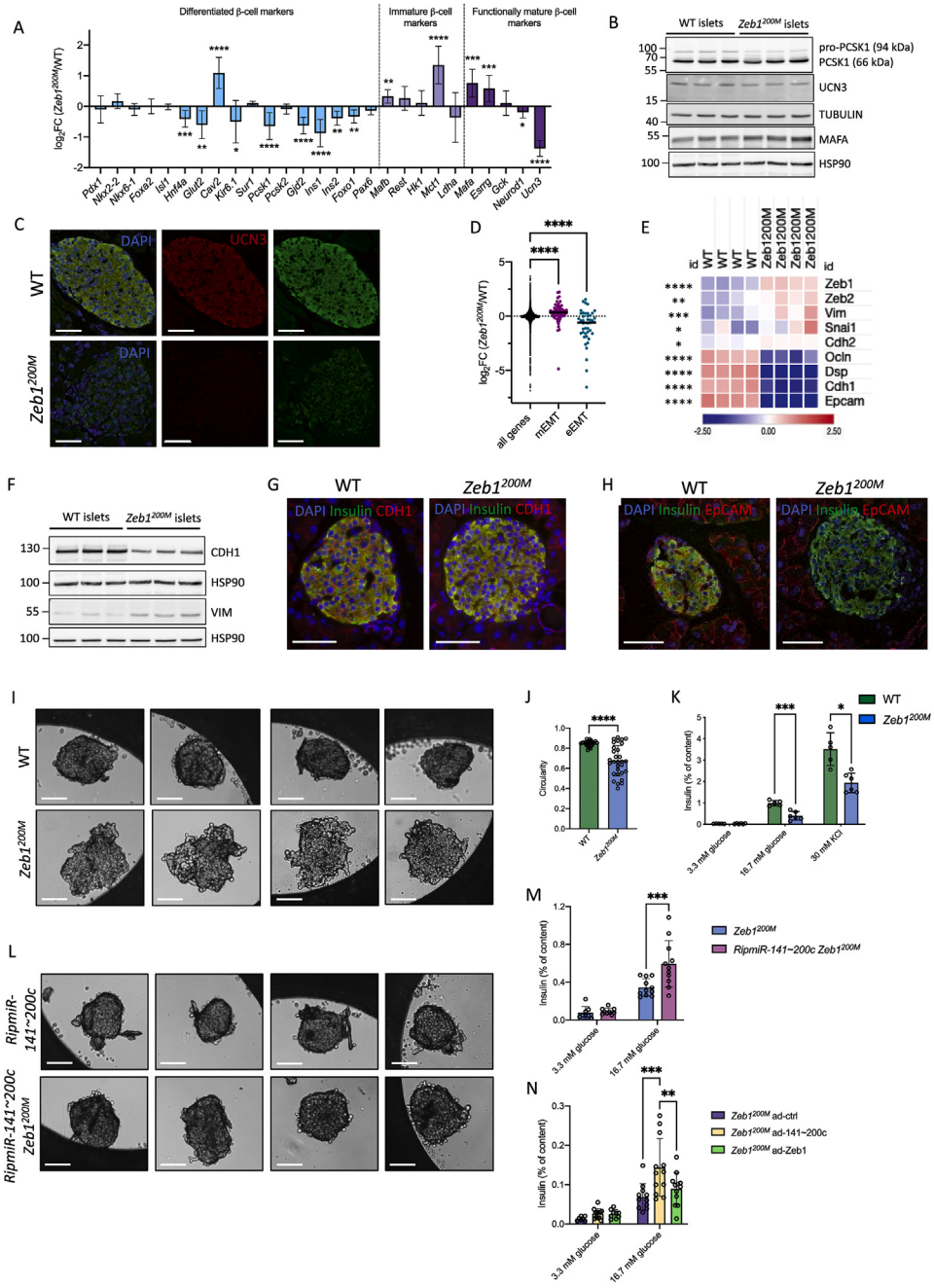

Figure 2: *Zeb1*^{200} mutation drives partial β-cell dedifferentiation and promotes EMT gene expression program in unstressed islets. **(A)** log_2FC and P-values of selected transcripts in *Zeb1*^{200M} vs. WT islets pertaining to β-cell differentiation and maturity. **(B)** Immunoblotting of PCSK1, UCN3, MAFA, and loading controls HSP90 and TUBULIN in WT and *Zeb1*^{200M} islets (n = 1–2 mice per well). **(C)** Representative confocal images of immunofluorescence staining of UCN3 and insulin expression in WT and *Zeb1*^{200M} islets. Scale bar = 50 μm. **(D)** log_2FC of mesenchymal EMT genes (mEMT) and epithelial EMT genes (eEMT) in *Zeb1*^{200M} vs. WT islets. **(E)** Heatmap depicting log_2FC and P-values of selected EMT transcripts in WT and *Zeb1*^{200M} islets. **(F)** Immunoblotting of CDH1, VIM, and loading control HSP90 in WT and *Zeb1*^{200M} islets (n = 1–2 mice per well). **(G)** Representative immunofluorescence staining of insulin and CDH1 in WT and *Zeb1*^{200M} islets. Scale bar = 50 μm. **(H)** Representative confocal images of immunofluorescence staining of insulin and EpCAM in WT and *Zeb1*^{200M} islets. Scale bar = 50 μm. **(I)** Representative brightfield microscopy images of reaggregated WT and *Zeb1*^{200M} islets. Scale bar = 62 μm. **(J)** Quantification of circularity as a measure of aggregation efficiency of WT and *Zeb1*^{200M} reaggregated islets (n = 26–30 reaggregated islets). **(K)** Insulin secretion expressed as % of the content of reaggregated WT and *Zeb1*^{200M} islets following exposure to high glucose and KCl (n = 5–6). **(L)** Representative brightfield microscopy images of reaggregated *RipmiR-141~200c* and *RipmiR-141~200c Zeb1*^{200M} islets. Scale bar = 62 μm. **(M)** Insulin secretion expressed as % of the content of reaggregated *RipmiR-141~200c Zeb1*^{200M} and *Zeb1*^{200M} islets following exposure to high glucose (n = 11). **(N)** Insulin secretion expressed as % of the content of reaggregated *Zeb1*^{200M} islets transduced with control, miR-141–200c, or *Zeb1* adenovirus during the reaggregation process and stimulated with high glucose (n = 11–12). **Data information: (A, D–E)** RNA sequencing of *Zeb1*^{200M} vs. WT islets, n = 4, 13–15 weeks of age. Data are plotted as **(A)** mean ± 95% confidence intervals and **(D)** mean with an overlay of log_2FC of individual transcripts, **(J–K, M–N)** mean ± SD. Significance was evaluated by quasi-likelihood differential expression test **(A, E)**, Kruskal–Wallis test followed by Dunn's multiple comparisons test **(D)**, unpaired t-test **(J)**, and two-way ANOVA followed by Sidak's multiple comparisons test **(K, M–N)**. *P ≤ 0.05; **P ≤ 0.01; ***P ≤ 0.001; ****P ≤ 0.0001.

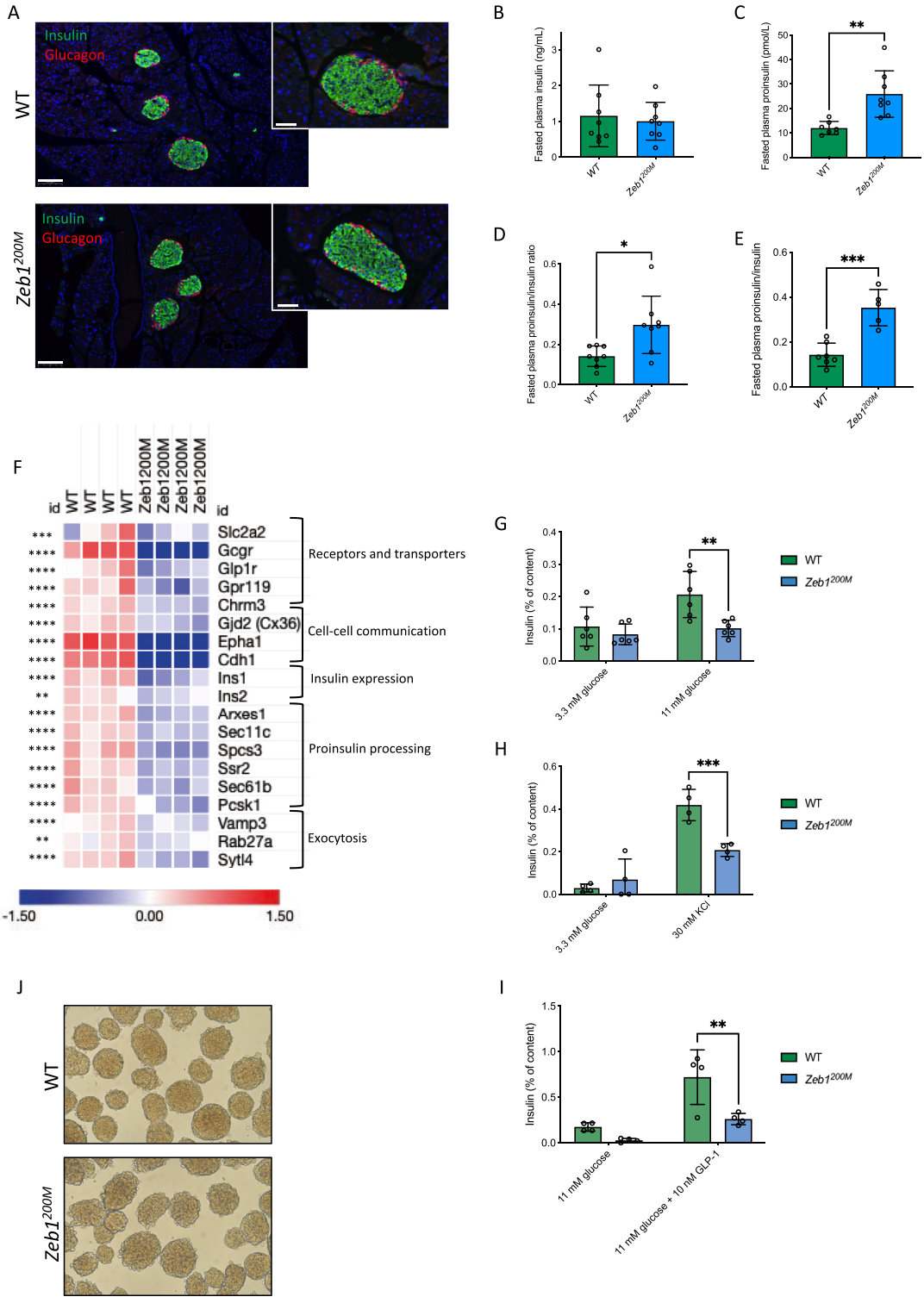

Figure 3: *Zeb1*^{200M} mice have increased circulating proinsulin, and *ex vivo Zeb1*^{200M} islets have defective insulin secretion. (A) Representative immunofluorescence staining of insulin and glucagon in WT and *Zeb1*^{200M} islets. Scale bar = 100 μm left, 50 μm right. Signal intensity has been boosted to reveal islet morphology. **(B–E)** Fasted plasma **(B)** insulin and **(C)** proinsulin levels and **(D)** proinsulin/insulin ratio in adult mice and **(E)** aged mice (60 weeks). **(F)** Heatmap depicting $\log_2$FC and P-values of genes involved in different aspects of insulin secretion in WT and *Zeb1*^{200M} islets. **(G–I)** *Ex vivo* insulin secretion assays of WT and *Zeb1*^{200M} islets exposed to **(G)** high glucose, **(H)** KCl, and **(I)** GLP-1. **(J)** Representative microscopy image of isolated WT and *Zeb1*^{200M} islets (100x). **Data information: (F)** RNA sequencing of *Zeb1*^{200M} vs. WT islets, n = 4, 13–15 weeks of age. **(B–E, G–I)** Data are plotted as mean ± SD. Significance was evaluated by a two-tailed t-test **(B–E)**, quasi-likelihood differential expression test **(F)**, and two-way ANOVA followed by Sidak's multiple comparisons test **(G–I)**. *P ≤ 0.05; **P ≤ 0.01; ***P ≤ 0.001; ****P ≤ 0.0001.

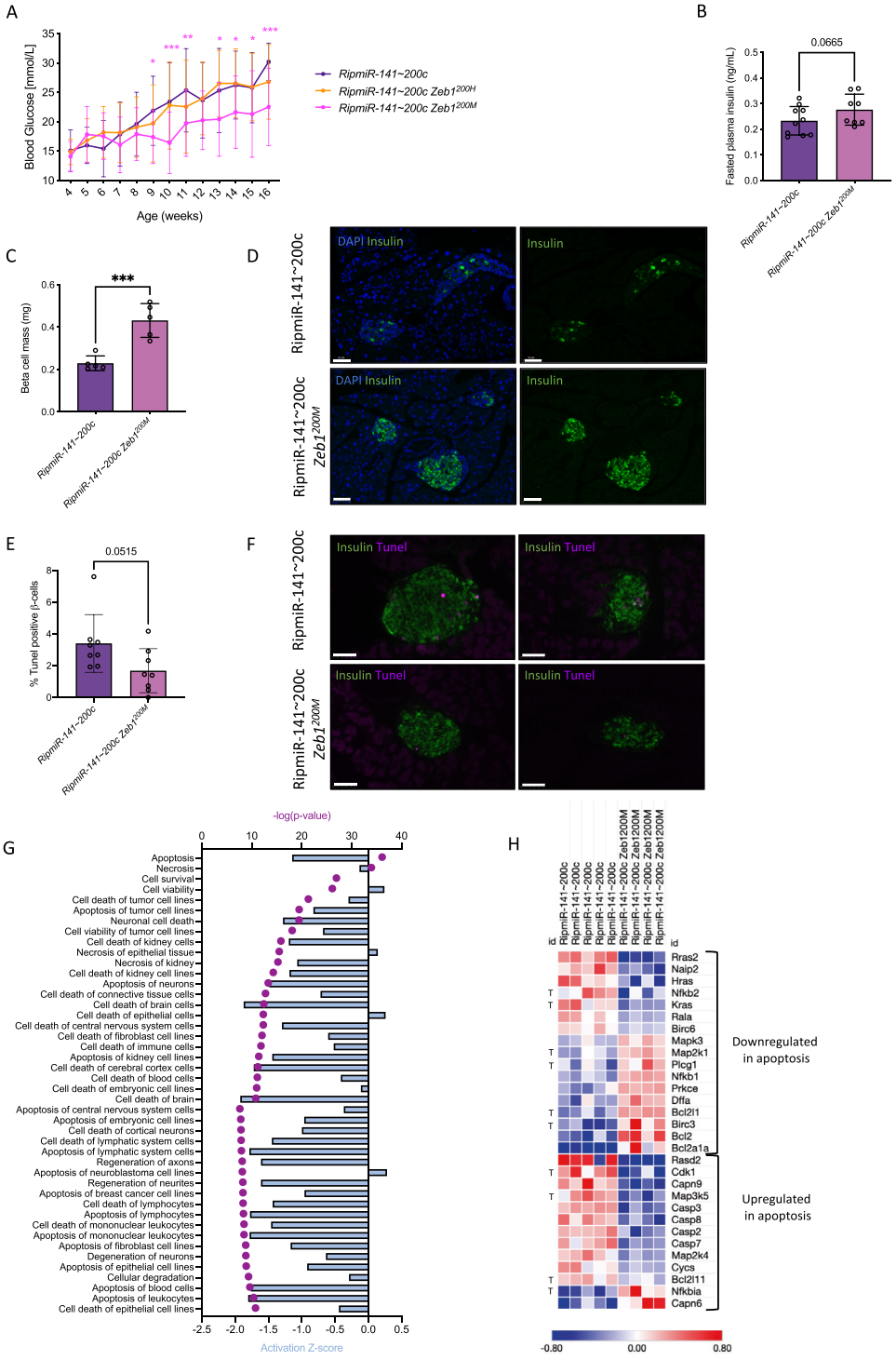

Figure 4: *Zeb1*^{200} mutation partially inhibits miR-141~200c-induced apoptosis. (A) Longitudinal random fed blood glucose measurements of *RipmiR-141~200c, RipmiR-141~200c Zeb1*^{200H}, and *RipmiR-141~200c Zeb1*^{200M} mice (n = 22, 14, 13, respectively). **(B)** Fasted plasma insulin of *RipmiR-141~200c* and *RipmiR-141~200c Zeb1*^{200M} mice (n = 8–10, 18 weeks of age). **(C)** β-cell mass of *RipmiR-141~200c* and *RipmiR-141~200c Zeb1*^{200M} mice (n = 5 mice, 18 weeks of age). **(D)** Representative insulin immunofluorescence staining in pancreatic sections of 18-week-old *RipmiR-141~200c* and *RipmiR-141~200c Zeb1*^{200M} mice. **(E)** % Tunel-positive β-cells in *RipmiR-141~200c* and *RipmiR-141~200c Zeb1*^{200M} islets (n = 8 pancreatic sections, 6 weeks of age). **(F)** Representative Insulin/TUNEL immunofluorescence staining in pancreatic sections of 6-week-old *RipmiR-141~200c* and *RipmiR-141~200c Zeb1*^{200M} mice. **(G)** Subcategories of top-ranked molecular and cellular function "cell death and survival" derived from Ingenuity analysis and ranked by P-value in *RipmiR-141~200c Zeb1*^{200M} vs. *RipmiR-141~200c* islets. **(H)** Significantly regulated apoptosis signaling genes in *RipmiR-141~200c Zeb1*^{200M} vs. *RipmiR-141~200c* islets. "T" depicts genes that are putative Zeb1 target genes. **Data information: (G–H)** RNA sequencing of *RipmiR-141~200c Zeb1*^{200M} vs. *RipmiR-141~200c* islets, n = 4–5, 6 weeks of age. **(A–C, E)** Data are plotted as mean ± SD. Significance was evaluated by two-way ANOVA followed by Dunnett's multiple comparisons test **(A)**, one-tailed t-test (**B**), and two-tailed t-test **(C, E)**. *P ≤ 0.05; **P ≤ 0.01; ***P ≤ 0.001; ****P ≤ 0.0001.

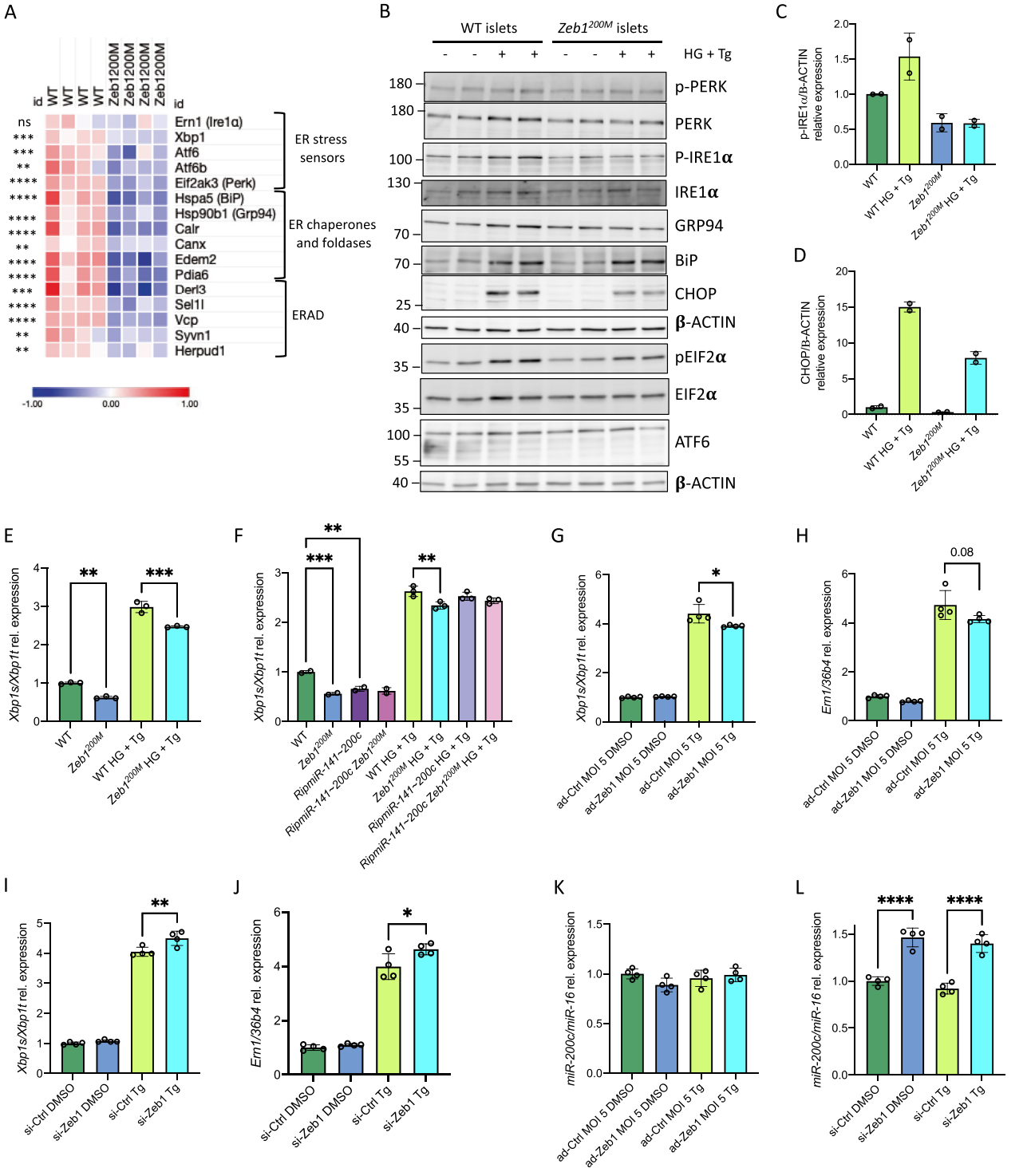

Figure 5: *Zeb1*^{200} mutation blunts ER stress signaling. (A) Heatmap depicting log_2FC and P-values of ER stress sensors, ER chaperones, and ERAD components in WT and *Zeb1*^{200M} islets. **(B)** Western blots showing induction of ER stress signaling in WT and *Zeb1*^{200M} islets (n = 6–8 mice per genotype, pooled) cultured with high glucose for 48 h followed by thapsigargin (Tg) treatment (6 h for upper 8 blots, 20 h for lower 4 blots). **(C–D)** Western blot densitometry quantification of **(C)** pIRE1α/β-ACTIN and **(D)** CHOP/β-ACTIN. **(E–F)** qPCR measurement of *Xbp1* splicing in islets treated with high glucose (48 h) and Tg (6 h) via quantification of spliced *Xbp1 (Xbp1s)* over total *Xbp1 (Xbp1t)* in **(E)** islets of WT and *Zeb1*^{200M} mice (n = 4 mice per genotype, pooled) and **(F)** islets of WT, *Zeb1*^{200M}, *RipmiR-141~200c* and *RipmiR-141~200c Zeb1*^{200M} littermate mice (n = 2–5 mice per genotype, pooled). **(G–L)** qPCR measurement of **(G)** *Xbp1s*/*Xbp1t*, **(H)** *Ern1/36b4*, and **(K)** *miR-200c/miR-16* in INS-1E cells transduced with control adenovirus or *Zeb1*-overexpressing adenovirus and treated with DMSO or Tg (6 h); and **(I)** *Xbp1s*/*Xbp1t*, **(J)** *Ern1/36b4* **(L)** *miR-200c/miR-16* in INS-1E cells transfected with control siRNA or *Zeb1*-siRNA and treated with DMSO or Tg (n = 4). **Data information: (A)** RNA sequencing of *Zeb1*^{200M} vs. WT islets, n = 4, 13–15 weeks of age. **(C–L)** Data are plotted as mean ± SD. Significance was evaluated by quasi-likelihood differential expression test **(A)**, and one-way ANOVA followed by Tukey's multiple comparisons test **(E–J)**, with significance only shown for most relevant comparisons. P > 0.05; *P ≤ 0.05; **P ≤ 0.01; ***P ≤ 0.001; ****P ≤ 0.0001.

(ThermoFisher). Library preparation was performed using the TruSeq Stranded mRNA Library Prep Kit (Illumina). For *RipmiR-141~200c Zeb1^{200M}* vs. *RipmiR-141~200c*, RNA was extracted from islets isolated from 6-week-old mice using TRI-Reagent (Sigma—Aldrich), followed by purification using the Picopure RNA Isolation kit (ThermoFisher). Library preparation was performed using the Smartseq II kit (Illumina). Libraries were sequenced on an Illumina Novaseq 6000 at the Functional Genomics Center Zürich (FGCZ).

2.17. Data availability

RNA sequencing data of *Zeb1^{200M}* vs. WT islets and *RipmiR-141~200c Zeb1^{200M}* vs. *RipmiR-141~200c* islets are available at ArrayExpress under accession numbers E-MTAB-10535 and E-MTAB-10537, respectively.

2.18. Statistical analysis

Statistical analysis was performed using GraphPad Prism 9.0. Data are represented as mean ± SD unless otherwise stated. Details regarding statistical tests used and biological and technical replicates are indicated in the respective figure legends. Statistical significance is indicated as * $P \leq 0.05$; ** $P \leq 0.01$; *** $P \leq 0.001$; **** $P \leq 0.0001$. Animals in experiments were age-matched, and littermates were used whenever possible.

2.19. Bioinformatic analysis

RNA sequencing data analysis was performed by the Functional Genomics Center Zürich. In brief, raw reads were cleaned by removing adapter sequences, trimming low-quality ends, and filtering low-quality reads (phred quality <20) using Trimmomatic (Version 0.36) [35]. The sequence pseudo alignment of the resulting high-quality reads to the mouse reference genome (GRCm38.p6) and gene level expression quantification (gene models from GENCODE release M32) were carried out using Kallisto (version 0.44) [36]. Differentially expressed genes were identified using R package edgeR (Bioconductor, Version 3.10) [37] by using a generalized linear model (glm) regression, a quasi-likelihood (QL) differential expression test, and the trimmed means of M-values (TMM) normalization. Pathway enrichment analysis and upstream regulator analysis were performed using Ingenuity (Qiagen). Motif analysis of *Zeb1^{200M}* vs. WT sequencing data was performed using ISMARA [38]. Predicted miR-200c and miR-141 target genes were identified using Targetscan v6.2 [29,30]. Heatmaps were generated using the online tool Morpheus (Broad Institute, https://software.broadinstitute.org/morpheus) and represent the log_2FC of normalized counts of individual samples vs. the average normalized counts for each gene.

3. RESULTS

3.1. Mutation of miR-200-binding sites in *Zeb1* leads to regulation of the miR-200—Zeb1 feedback loop and strong transcriptional changes in unstressed islets

To better understand the function of *Zeb1* in β-cells and define its contribution to miR-200-mediated phenotypes, we performed transcriptional analysis of islets isolated from mice homozygous for the *Zeb1^{200}* mutation (*Zeb1^{200M}*) and WT littermates. We identified 2408 downregulated and 2212 upregulated genes, with the highest amplitude fold-change among downregulated genes (Figure 1A). *Zeb1* mRNA levels increased ~2-fold ($log_2FC = 0.989$, $p = 5.116e\text{-}09$) (Figure 1B) and ZEB1 protein levels increased ~6-fold (Figure 1C, Supplemental Figure 1A), confirming *Zeb1* derepression upon the mutation of its endogenous miR-200-binding sites. Significantly regulated canonical functions determined by Ingenuity analysis included terms relating to insulin secretion signaling, epithelial adherens junctions, unfolded protein response, endoplasmic reticulum stress pathway, and oxidative stress response, all with negative Z-scores signifying decreased activity (Figure 1D, Supplemental Figure 1B).

An analysis of an existing ChIP dataset performed in epithelial cells [39] showed significant downregulation of putative ZEB1 target genes in *Zeb1^{200M}* vs. WT islets (Figure 1E), consistent with ZEB1's primary role as a transcriptional repressor [40,41]. Though *Zeb1* is a direct target of miR-200, it also binds to E-box and Z-box domains in the promoter regions of both miR-200 genomic clusters and decreases their expression, effectively engaging in a double-negative feedback loop with the miR-200 family [22—24] (Figure 1F). As previously observed in an insulinoma mouse model [25], *Zeb1* overexpression driven by homozygous *Zeb1^{200}* mutation led to a strong repression of all 5 members of the miR-200 family but not of control miR-16 (Supplemental Figure 1C—H). As a result, the predicted target genes harboring miR-200c and miR-141 seed regions were derepressed (Figure 1G—H). Interestingly, unbiased analysis of all differentially expressed genes in *Zeb1^{200M}* vs. WT islets using ISMARA, which identifies key transcription factors and miRNAs driving gene expression changes [38], ranked ZEB1 as the top regulator and the miR-200b/200c/429 seed in the second position, while the miR-141/200a seed was only in position 44 (Supplemental Figure 1I). This result confirmed the more potent role of the miR-200c seed compared to the miR-141 seed in this context, which was also reflected in the target gene derepression (Figure 1G—H) and previously observed in islets and insulinomas [16,25]. In summary, dissociation of *Zeb1* from the repressive function of the miR-200 family in unstressed islets led to strong and consistent transcriptional changes affecting multiple aspects of β-cell biology, likely resulting from regulation of both direct *Zeb1* target genes and the secondary regulation of miR-200 target genes by ZEB1 via the double-negative feedback loop.

3.2. *Zeb1^{200}* mutation drives partial β-cell dedifferentiation and promotes EMT gene expression program in unstressed islets

Based on the well-studied role of *Zeb1* in regulating EMT and dedifferentiation in cancer [21,42], we next focused on those pathways in unstressed islets. In *Zeb1^{200M}* islets, expression levels of some critical β-cell differentiation markers were significantly reduced compared to WT islets, including *Hnf4α*, *Glut2*, *Kir6.1*, *Pcsk1*, *Gjd2 (Cx36)*, *Ins1*, *Ins2*, and *Foxo1*, indicating a partial loss of identity [43,44]. In addition, *Mafb* and *Mct1*, which are enriched in immature neonatal β-cells compared to mature adult β-cells [45], were more highly expressed in adult *Zeb1^{200M}* vs. WT islets, whereas *Ucn3*, a marker of functional maturity in β-cells [43], was decreased to 38.5% of its WT levels, a gene expression pattern indicative of reduced functional maturation in *Zeb1^{200M}* islets (Figure 2A). Surprisingly, *Mafa* and *Esrrg*, two drivers of functional maturation of β-cells, were overexpressed in *Zeb1^{200M}* islets compared to WT. However, known targets of *Mafa*, including *Ins2, Slc2a2, Pdx1, Nkx6-1,* and *Pcsk1* [46], were either decreased in expression or not regulated, suggesting a lack of transcriptional consequences of this upregulation of *Mafa*. Transcriptional regulation of β-cell differentiation markers was further confirmed at the protein level by immunoblotting and immunofluorescence staining, revealing a decreased expression of pro-PCSK1 and mature PCSK1, UCN3, and Insulin expression in *Zeb1^{200M}* compared to WT islets, as well as a subtle increase in MAFA expression (Figure 2B—C; Supplemental Figure 2A—G). Together, these data reveal that *Zeb1^{200M}* islets express markers of partial dedifferentiation and reduced functional maturation compared to WT islets.

As described above, the miR-200 family and *Zeb1* negatively regulate each other transcriptionally (Figure 1F, Supplemental Figure 1C—H), obscuring the distinction between direct *Zeb1* functions and indirect functions via the miR-200 family. To resolve these two branches, we crossed the $Zeb1^{200}$ locus into *RipmiR-141~200c* mice that overexpress the miR-141—200c cluster in β-cells, which leads to an increase in the expression of miR-141 and miR-200c ~4—6 fold compared to WT animals [16]. Notably, the *RipmiR-141~200c* transgene is not subject to repression by ZEB1, enabling the generation of mice with derepressed *Zeb1* and a sustained expression of miR-200c and miR-141 (Supplemental Figure 2H—L), the two most highly expressed miRNAs of the miR-200 family [16]. In contrast to $Zeb1^{200M}$ vs. WT islets, expression levels of *Ins1, Ins2,* and other β-cell differentiation markers were not decreased in *RipmiR-141~200c* $Zeb1^{200M}$ vs. *RipmiR-141~200c* islets, while functional maturity markers were similarly deregulated (Supplemental Figure 2M). In relation to the miR-200—Zeb1 axis, this suggests that β-cell identity is controlled by miR-200 target genes other than *Zeb1*, while functional maturation is mainly dependent on ZEB1 target genes independent of the miR-200 family. This observation is in line with previous data in an insulinoma mouse model, in which tumors and metastases were more frequently insulin-positive upon miR-200-reexpression [25].

Analysis of core EMT genes obtained in a meta-analysis of 18 studies [47] in $Zeb1^{200M}$ vs. WT islets revealed a significant increase in the expression of EMT genes associated with a mesenchymal state (mEMT) and a significant decrease in the expression of genes associated with an epithelial state (eEMT; Figure 2D). Mesenchymal marker *Vim*, EMT-TFs *Zeb2* and *Snai1*, and mesenchymal cadherin *Cdh2* were significantly upregulated, while in parallel, epithelial junction proteins such as *Ocln*, *Cdh1*, *Epcam*, and *Dsp* were strongly downregulated in $Zeb1^{200M}$ islets, down to 27% (*Ocln*), 16% (*Cdh1*), or only 3% (*Epcam*, *Dsp*) of their WT mRNA levels (Figure 2E). Importantly, an increased expression of VIM and decreased expression of CDH1 and EpCAM were further confirmed at the protein level (Figure 2 F—H, Supplemental Figure 2 N—O). Interestingly, in the *RipmiR-141~200c* background, sustained miR-200 expression combined with $Zeb1^{200M}$ led to a less consistent increase in mEMT gene expression but a similar reduction in eEMT gene expression (Supplemental Figure 2P—Q). This finding is consistent with the direct repression of eEMT genes such as *Cdh1* and *Epcam* by ZEB1 [27,48] and is independent of miR-200 expression.

Several studies have shown that junctional proteins, particularly E-cadherin (CDH1), are crucial for the proper aggregation of β-cell lines into pseudoislets *in vitro* [49—51]. To determine whether the transcriptional changes in $Zeb1^{200M}$ islets perturb aggregation *in vitro*, we dispersed islets isolated from $Zeb1^{200M}$ and WT mice and reaggregated them using a hanging drop method, beginning with an equal number of cells (2000 cells). We utilized commercially available plates optimized to generate highly consistent, functional, and size-matched islet spheroids for this procedure. Dispersed $Zeb1^{200M}$ islet cells reaggregated into islets, though they had a looser, less defined appearance than reaggregated WT islets (Figure 2I). In line with their reduced aggregation and compaction, $Zeb1^{200M}$ reaggregated islets had a less circular shape than WT reaggregated islets (Figure 2J). Functionally, $Zeb1^{200M}$ reaggregated islets demonstrated impaired insulin secretion upon exposure to high glucose or KCl (Figure 2K), whereas basal insulin secretion and total insulin content were unchanged (Supplemental Figure 2R), confirming the importance of cell—cell contacts and adhesion in insulin secretion [52—54].

To further explore the role of miR-200 target genes vs. direct ZEB1 target genes in aggregation, we repeated this experiment starting from *RipmiR-141~200c* $Zeb1^{200M}$ and *RipmiR-141~200c* islets. Surprisingly, the overexpression of miR-200 (Supplemental Figure 2S—T) rescued the looser appearance of $Zeb1^{200M}$ reaggregated islets (Figure 2L) and increased insulin secretion (Figure 2M). These results suggest that though expression of key epithelial junction proteins, such as *Cdh1,* was strongly reduced in both $Zeb1^{200M}$ vs. WT islets and *RipmiR-141~200c* $Zeb1^{200M}$ vs. *RipmiR-141~200c* islets, other adhesion and junction proteins also play important roles in islet cell aggregation. Furthermore, numerous genes belonging to the Ingenuity term "cell adhesion," which were differentially expressed in $Zeb1^{200M}$ vs. WT islets, were not significantly regulated in *RipmiR-141~200c* $Zeb1^{200M}$ vs. *RipmiR-141~200c* islets (Supplemental Figure 2U—V), offering additional possible candidates that might explain the observed differences in aggregation.

Finally, we sought to determine whether miR-141—200c adenoviral transduction in dissociated $Zeb1^{200M}$ islets during reaggregation would lead to similar results. Treatment with adenovirus overexpressing miR-141—200c to levels similar to *RipmiR-141~200c* $Zeb1^{200M}$ reaggregated islets (Supplemental Figure 2S—T) led to no significant improvement in reaggregated islet appearance compared to control adenovirus or adenovirus expressing *Zeb1* (Supplemental Figure 2W). This finding is perhaps due to a developmental defect that could not be rescued by miR-200 overexpression in adult islets or the delay in adenoviral overexpression in relation to the early stages of the reaggregation process. However, we did detect a mild increase in insulin secretion upon *miR-141~200c* re-expression (Figure 2N), again confirming a role for the miR-200 family in regulating β-cell function.

3.3. $Zeb1^{200M}$ mice have increased circulating proinsulin, and *ex vivo* $Zeb1^{200M}$ islets have defective insulin secretion

The $Zeb1^{200}$ mutation led to many transcriptional changes in islets, inducing gene expression patterns indicative of partial dedifferentiation and EMT (Figure 2A—H) and suggestive of potential perturbation of insulin secretion and the unfolded protein response (UPR) (Figure 1D). Therefore, we sought to determine the *in vivo* impact of the $Zeb1^{200M}$ mutation in a metabolic context. Immunofluorescence staining of $Zeb1^{200M}$ and WT pancreatic sections revealed no apparent change in islet morphology or the distribution of α- and β-cells (Figure 3A), suggesting no major developmental defects of the endocrine pancreas were due to *Zeb1* overexpression. In addition, β-cell-mass was unchanged (Supplemental Figure 3A). $Zeb1^{200M}$ mice displayed no significant metabolic changes: longitudinal blood glucose and body weight were unaltered (Supplemental Figure 3B—C), and glucose tolerance, insulin tolerance, and pyruvate tolerance were normal (Supplemental Figure 3D—G). Interestingly, while $Zeb1^{200M}$ mice had normal fasted plasma insulin levels (Figure 3B), they had significantly higher proinsulin levels (Figure 3C—D), an effect that became more pronounced with age (Figure 3E), suggesting a defect in proinsulin processing.

Ingenuity analysis of $Zeb1^{200M}$ vs. WT islet RNA sequencing data identified the "insulin secretion signaling pathway" as the canonical function with the most significant p-value and assigned it a negative Z-score (Supplemental Figure 1B). In line with the observed increase in plasma proinsulin in $Zeb1^{200M}$ mice (Figure 3C—E), $Zeb1^{200M}$ islets had decreased expression of several genes involved in proinsulin processing, including prohormone convertase *Pcsk1* and components of the SSR and Sec61 translocon, involved in the translocation of pre-proinsulin into the ER (Figure 3F) [55]. In addition, transcripts in other components of the insulin secretion signaling pathway had decreased expression as well, including glucose transporter *Glut2 (Slc2a2)*, junctional components such as *Cx36* and *Cdh1* that are key for cell—cell communication in a coordinated insulin secretion response, and

exocytosis-related genes such as *Rab27a* (Figure 3F) [53,56]. To determine the *in vivo* effects of the *Zeb1*^{200M} mutation on insulin secretion, we injected fasted *Zeb1*^{200M} and WT mice with a glucose bolus and measured plasma insulin 15 and 30 min later. Insulin levels before and after glucose injection were similar in *Zeb1*^{200M} and WT mice, suggesting no defect in *in vivo* insulin secretion, and thus, likely reflecting an ability for the islets to compensate for these deficiencies (Supplemental Figure 3H—I). Intriguingly, insulin secretion from isolated islets was reduced in *Zeb1*^{200M} islets upon high glucose, KCl, and GLP-1 treatment compared to WT islets (Figure 3G—I), in line with the transcriptional perturbations of the insulin secretory network and the reduced expression of *Glut2* and *Glp1r* (Figure 3F). Of note, isolated islets from *Zeb1*^{200M} mice exhibited a less defined appearance than WT islets, suggesting that the isolation process may exacerbate junctional defects mediated by *Zeb1* overexpression, reducing cell—cell communication and contributing to defects in insulin secretion as observed with the reaggregated islets (Figures 3J and 2K).

3.4. *Zeb1*^{200} mutation partially inhibits miR-141—200c-induced apoptosis

In β-cells, it was previously shown that the *in vivo* overexpression of miR-141—200c under the rat insulin promoter (*RipmiR-141~200c*) leads to β-cell apoptosis and hyperglycemia in mice through the downregulation of a network of anti-apoptotic genes [16]. Interestingly, the derepression of *Zeb1* in this model (*RipmiR-141~200c Zeb1*^{200M}) led to a blunted increase in longitudinal blood glucose (Figure 4A), a mild increase in fasted plasma insulin (Figure 4B), and reduced body weight loss (Supplemental Figure 4A) compared to *RipmiR-141~200c* and *RipmiR-141~200c Zeb1*^{200H} mice (heterozygous for the *Zeb1*^{200} mutation). β-cell-mass was significantly higher in *RipmiR-141~200c Zeb1*^{200M} mice than in *RipmiR-141~200c* mice (Figure 4C—D), and TUNEL staining at 6 weeks of age suggested a mild decrease in the percent of apoptotic β-cells (Figure 4E—F). Ingenuity analysis of molecular and cellular functions of *RipmiR-141~200c Zeb1*^{200M} vs. *RipmiR-141~200c* islets identified "cell death and survival" as the top regulated function (Supplemental Figure 4B). Within this category, apoptosis was the most significantly regulated term and was assigned a negative Z-score, in support of a gene expression program of reduced apoptosis upon *Zeb1* mutation, while cell viability was also highly significant and assigned a positive Z-score (Figure 4G).

Mechanistically, only one of the four anti-apoptotic genes previously identified in the *RipmiR-141~200c* model [16] was significantly increased in expression (Supplemental Figure 4C). In contrast, two of the identified Trp53-targets, *Bax* and *Phlda3*, which were upregulated in *RipmiR-141~200c* vs. WT islets, were downregulated upon *Zeb1*^{200M} mutation (Supplemental Figure 4D). Though the regulation of these transcripts likely contributes to the observed reduction in apoptosis in *RipmiR-141~200c Zeb1*^{200M} islets, numerous additional apoptosis signaling genes were significantly regulated in *RipmiR-141~200c Zeb1*^{200M} vs. *RipmiR-141~200c* islets (Figure 4H), a majority in an anti-apoptotic manner, suggesting a more complex mechanism. Interestingly, some of these genes have been identified as putative *Zeb1* target genes in ChIP experiments (Figure 4H, marked with T) [39,57], while *Bcl2l11 (Bim)* has been demonstrated in particular to be a direct ZEB1 target involved in apoptosis resistance in cancer models [58,59].

3.5. Zeb1^{200} mutation blunts ER stress signaling

Ingenuity analysis of *Zeb1*^{200M} vs. WT islet RNA-sequencing data identified the UPR and ER stress response pathways as two significantly regulated canonical functions with negative Z-scores (Figure 1D). Independently, unbiased causal analysis of all transcriptional changes in *Zeb1*^{200M} vs. WT islets using Ingenuity ranked *Xbp1* as the top upstream regulator of this dataset, with an activation Z-score of −8.468 and p-value of 1.99e-44. Transcriptional analysis of unstressed *Zeb1*^{200M} vs. WT islets revealed significantly decreased expression of transcripts at all levels of the ER stress response pathway. At the level of ER stress sensing, all 3 branches (*Ire1α-Xbp1*, *Atf6*, and *Eif2ak3/Perk*) had reduced expression. ER chaperones such as *Hspa5* (*BiP*), *Pdia6*, and *Calr*, which have known roles in proinsulin folding [60], and ERAD components including *Derl3* and *Sel1l* were also reduced in expression (Figure 5A, Supplemental Figure 5A). This decrease in the expression of UPR genes and folding machinery may explain the increased circulating plasma proinsulin levels in *Zeb1*^{200M} vs. WT mice (Figure 3C—E). Interestingly, *RipmiR-141~200c Zeb1*^{200M} mice also had an increased ratio in fasted circulating proinsulin/insulin levels compared to *RipmiR-141~200c* mice, suggesting that Zeb1 targets other than miR-200 contribute to this defect in proinsulin processing (Supplemental Figure 5B).

All the transcriptional patterns described above occurred in unstressed islets, suggesting that subjecting *Zeb1*^{200M} and WT islets to ER stress may reveal relevant functional consequences. Treatment of islets with thapsigargin (Tg), a commonly used ER-stress inducer, led to the blunted activation of IRE1α, GRP94, EIF2α, and CHOP in *Zeb1*^{200M} islets compared to WT islets (Figure 5B—D, Supplemental Figure 5C—J) and reduced *Xbp1* splicing measured by a decrease in spliced *Xbp1* (*Xbp1s*) over total *Xbp1* (*Xbp1t*; Figure 5E) [61]. Thus, in accordance with the transcriptional changes described, *Zeb1*^{200M} islets displayed resistance to chemically induced ER stress. Intriguingly, in the *RipmiR-141~200c* background, the decreased *Xbp1* splicing upon *Zeb1*^{200} mutation was lost (Figure 5F), suggesting the resistance to ER stress is, at least partially, mediated via ZEB1 regulation of miR-200.

To confirm that ZEB1 directly regulates *Xbp1* splicing, we manipulated *Zeb1* levels in the INS1E β-cell line, followed by Tg treatment. The overexpression of *Zeb1* led to a mild decrease in *Xbp1* splicing and a downward trend in *Ern1* (*Ire1α*) expression (Figure 5G—H, Supplemental Figure 5K), whereas *Zeb1*-knockdown (KD) led to the inverse effect, notably increased *Xbp1* splicing and increased *Ern1* expression (Figure 5I—J, Supplemental Figure 5L). To determine the dependency on miR-200 in these scenarios, we further quantified the expression levels of the miR-200 family. *Zeb1* overexpression did not downregulate miR-200c, miR-141, or miR-200a expression in these experimental conditions (Figure 5K, Supplemental Figure 5M—N), presumably due to the stability of mature miRNAs, whereas *Zeb1*-KD led to the derepression of miR-200c, miR-141, and miR-200a (Figure 5L, Supplemental Figure 5O—P). These results, generated in a transformed β-cell line, emphasize that the miR-200—Zeb1 axis regulates the response to ER stress in a cell-autonomous manner and that this regulation is likely mediated by both miR-200 target genes and ZEB1 target genes.

4. DISCUSSION

Although the miR-200—Zeb1 axis has been extensively studied in the context of cancer progression, studies in the realm of pancreatic islets and metabolism are scarce. Here we sought to determine the role of *Zeb1* in islet development, function, and survival by dissociating it from its repressor, the miR-200 family. Genetic mutation of all miR-200 binding sites in the *Zeb1* 3′UTR induced an upregulation of *Zeb1* expression ≈2-fold in murine β-cells, which was sufficient to induce extensive and consistent transcriptional changes in islets, affecting key pathways such as insulin secretion, cell—cell junction remodeling and

signaling, and ER stress response. Interestingly, in unstressed conditions, these transcriptional changes did not lead to pronounced morphological or metabolic consequences *in vivo*, demonstrating the remarkable plasticity and extraordinary ability of islets to compensate and maintain their function. In contrast, in pro-apoptotic conditions, *Zeb1* overexpression provided a protective effect.

A few previous studies have examined the function of the miR-200—Zeb1 axis in islets. miR-200 levels are overexpressed in *ob/ob* mice [16,17], in parallel with a decrease in *Zeb1* expression [17]. Furthermore, the overexpression of the miR-141—200c cluster *in vivo* induced β-cell apoptosis [16], concurring with *in vitro* data demonstrating that the overexpression of miR-200b or *Zeb1*-KD induces apoptosis in INS-1 cells [17]. Inhibition of *miR-141~200c* expression led to a reduction in luciferase activity of an insulin reporter [62], and a recent study identified miR-200a as a key regulator of β-cell differentiation [18]. Finally, increased *Zeb1* expression was associated with EMT in the *in vitro* expansion of human islets [11]. Therefore, our results are in concordance with previous studies and add to the role of the miR-200—Zeb1 axis in β-cell function, differentiation, and survival. We further identify novel functions of the miR-200—Zeb1 axis in regulating aggregation, UPR, and the ER stress response in islets.

Distinguishing the respective contributions of the miR-200 and Zeb1 branches of the miR-200—Zeb1 axis is complicated by their involvement in a double-negative feedback loop [22,23]. This loop has primarily been studied in a cancer context [25,63] and is, therefore, interesting to observe that in unstressed conditions, a ≈2-fold increase in *Zeb1* expression leads to a profound downregulation of all five miR-200 family members by ≈ 90%. To distinguish functions of direct ZEB1 target genes and miR-200 target genes indirectly regulated via the feedback loop, we studied the pathways identified in $Zeb1^{200M}$ vs. WT islets in the *RipmiR-141~200c* background, in which *miR-141~200c* is re-expressed and not subject to repression by ZEB1. Some transcriptional patterns, such as strongly reduced *Cdh1* and *Epcam* expression, were maintained in the *RipmiR-141~200c* background, whereas others such as reduction of *Ins1* and *Ins2* expression were lost. Furthermore, reduced *Xbp1* splicing upon thapsigargin treatment of $Zeb1^{200M}$ vs. WT islets was also lost, whereas apoptosis resulting from *miR-141~200c* overexpression in β-cells was partially mitigated via $Zeb1^{200}$ mutation. The results of this study suggest that *Zeb1* function in β-cells is exerted via a combination of direct ZEB1 target genes (other than miR-200) and indirect regulation of miR-200 target genes. In reality, the complexity of regulation is even more intricate, as ZEB1 has also been found to regulate the expression of numerous other miRNAs, either by binding their promoters directly (i.e., miR-1199) or indirectly (i.e., miR-34a). Intriguingly, miR-34a likely plays a role in β-cell apoptosis [64,65], thus confirming the potential relevance of these additional layers of regulation in β-cell function and survival.

The high sensitivity and evolutionary conservation of the miR-200—Zeb1 double-negative feedback loop reflect its important biological function. Double-negative feedback loops are particularly powerful in reinforcing and maintaining the establishment of either state in a bistable system [66]. Interestingly, several examples of double-negative feedback loops between miRNAs and transcription factors involved in the regulation of developmental processes and differentiation exist, reflecting evolutionary pressure for network motifs that combine both post-transcriptional and transcriptional regulation [67]. For the miR-200—Zeb1 loop and EMT, miR-200 promotes an epithelial state, and ZEB1 promotes a mesenchymal state; due to the reinforcing activity of this double-negative feedback loop, an upstream signal can more efficiently induce a shift into either state [23]. In contrast to some double-negative feedback loops [67,68], the miR-200—Zeb1 double-negative feedback loop is reversible, conferring a certain degree of plasticity depending on the stimulus [23,24], which is important in the context of EMT. Though EMT plays critical roles in establishing the mesenchymal cell fate during embryonic development [69], it is also involved in keratinocyte migration and re-epithelialization during wound healing [26], a process that requires reversibility to return to the original epithelial state. In the context of islets and differentiation, the reversibility of the miR-200—Zeb1 feedback loop may enable adult mature β-cells to undergo mild dedifferentiation in order to proliferate during pregnancy- or obesity-associated β-cell compensation, before reverting to a more mature state. This finding would be in line with previous observations *in vivo* and *in vitro* that proliferating β-cells have decreased expression of β-cell identity and maturity markers [70—72]. A comparative transcriptomic analysis of WT and $Zeb1^{200M}$ islets revealed gene expression patterns indicative of EMT, dedifferentiation, and defects in insulin secretion, all of which could lead to perturbations in islet morphology and function. EMT is thought to be involved in the development of mouse, sheep, and human endocrine pancreases and coalescence of islets [73,74]. The function of Cdh1, the most highly expressed cadherin in islets and a direct target of ZEB1, has been studied: specifically, overexpression of a dominant-negative truncated CDH1 mutant was found to perturb islet formation *in vivo* [75]. Two later loss-of-function studies, however, demonstrated that *Cdh1* was dispensable for proper islet formation [76,77]. In support of the latter two studies, $Zeb1^{200M}$ mice had morphologically normal islets, despite a strong downregulation of *Cdh1*, pointing toward a likely compensatory mechanism by other adhesion proteins. In the context of β-cell identity and function, despite downregulation of key β-cell differentiation markers and gene expression patterns indicative of functional immaturity and insulin secretory defects in islets, $Zeb1^{200M}$ mice had normal blood glucose and insulin levels and displayed no impairment in insulin secretion *in vivo.* Therefore, it seems that β-cells can compensate for a certain degree of dedifferentiation *in vivo.* Understanding the mechanisms of dedifferentiation and its functional consequences is highly relevant, as β-cell-dedifferentiation is thought to complement apoptosis as a mechanism for the loss of functional β-cell-mass, contributing to hyperglycemia in T2D [4]. Furthermore, β-cell-dedifferentiation is important in the field of β-cell transplantation, as *in vitro* expansion of human β-cells has been shown to lead to dedifferentiation [10,11,78,79]. Notably, in line with the results of this study, increased *Zeb1* and *Zeb2* were found in dedifferentiating human islets in culture [11], while miR-200a drives β-cell differentiation [18], thus supporting the role of the miR-200—Zeb1 axis as an important regulator of β-cell identity.

One intriguing result of this study was that the defect in the aggregation of dissociated $Zeb1^{200M}$ islets was lost in the *RipmiR-141~200c* background. Zeb1 has been thoroughly studied as a driver of EMT, notably via its direct repression of epithelial junction proteins such as *Cdh1* and *Epcam* [27,48]. Importantly, the strong downregulation of these transcripts and other epithelial adhesion proteins by the $Zeb1^{200M}$ mutation was maintained in the *RipmiR-141~200c* background, confirming their direct repression by ZEB1. The function of Cdh1 has been studied in the context of aggregation and insulin secretion. Several studies demonstrated that the aggregation of Min6 cells into pseudoislets was perturbed by an antibody blockade of CDH1 [50,51] or antisense inhibition [49]. Though we also observed a disruption of reaggregation of islets with overexpressed *Zeb1* and reduced *Cdh1*, this effect was lost upon *miR-141~200c* overexpression, whereas *Cdh1* was still strongly repressed. This result suggests the importance of the many other adhesion proteins expressed in islets in *in vitro*

aggregation and of the involvement of the miR-200 family in their regulation. In addition, cell—cell junctions and intraislet communication have also been found to be key for a coordinated insulin secretion response [52]: Min6 cells have improved glucose-stimulated insulin secretion (GSIS) when grown as pseudoislets compared to adherent culture [51], whereas dispersed islets have impaired GSIS compared to native or reaggregated islets [80]. More specifically, higher *Cdh1* expression has been found to be correlated with increased GSIS in individual β-cells [81], and β-cell-KO of *Cdh1* leads to mild glucose intolerance and defective insulin secretion in mice [76]. In our study, *Zeb1*^{200M} mice had normal glucose tolerance, possibly because *Cdh1* was downregulated but not completely silenced. However, our findings of impaired insulin secretion in poorly reaggregated *Zeb1*^{200M} islets support the importance of cell—cell contact and junctional proteins such as CDH1 in β-cell function.

Perturbation of the miR-200—Zeb1 axis in β-cells led to the transcriptional downregulation of genes involved in many aspects of the ER stress signaling pathway, including ER stress sensors, ER chaperones, and ERAD components. Defective insulin processing in *Zeb1*^{200M} mice, as revealed by their increased circulating proinsulin levels compared to WT littermates, may have impaired initiation of the UPR due to a lack of sensing, as further demonstrated by the blunted activation of IRE1α-XBP1, EIF2α, and CHOP in *Zeb1*^{200M} islets treated with thapsigargin. This finding may seem paradoxical, as a functional UPR is thought to alleviate ER stress in islets [82,83], and elevated proinsulin levels are commonly associated with T2D [84]. In this case, however, reduced insulin expression in *Zeb1*^{200M} vs. WT islets (Figure 2A,C; Supplemental Figure 2F) may help to alleviate the low-level ER stress typically experienced by β-cells due to high insulin production, as previously demonstrated in mice with tamoxifen-induced insulin knockout [85], and that a mild defect in the sensing of misfolded proteins may be advantageous by preventing the progression of chronic ER stress to a pro-apoptotic response. It is also relevant to note that *Chop* ablation in the Akita model of β-cell ER stress reduced β-cell apoptosis and delayed hyperglycemia [86], suggesting that apoptosis in this model is related to pro-apoptotic ER stress signaling and not to the presence of the misfolded insulin itself.

Another relevant aspect to consider is how EMT and dedifferentiation are linked with ER stress. Chronic ER stress and failure of the adaptive UPR response in β-cells are thought to lead to T2D and β-cell dedifferentiation, as dedifferentiation may provide an escape from apoptosis [4]. The causative effect of EMT and dedifferentiation on the ER stress response, however, has not been investigated; this directionality is more relevant in the context of the *Zeb1*^{200M} model, as it is an increase in *Zeb1* expression that drives gene signatures of EMT and dedifferentiation, as well as decreased UPR and ER stress signaling. The UPR and ER stress responses are critical in β-cells, in which an elevated production of insulin, which comprises 30—50% of total protein synthesis in the β-cell, requires a high ER capacity for protein synthesis and folding [87,88], especially given the propensity of proinsulin to misfolding [89]. As a result, UPR genes are highly expressed in islets compared to other tissues [90]. Thus, it is conceivable that the loss of β-cell identity in the *Zeb1*^{200M} model led to a parallel loss of expression of UPR genes, as these cells expressed less insulin and became less β-cell-like. Interestingly, a similar phenomenon was observed in the *Tg7a2* mouse model, in which β-cell dedifferentiation and EMT are also associated with a loss in expression of many UPR genes [91]. Finally, another recent study found that miR-24 overexpression in Min6 cells led to an increased expression of β-cell dedifferentiation markers and resistance to thapsigargin-induced apoptosis [92].

Understanding the molecular mechanisms controlling dedifferentiation, EMT, and aggregation in β-cells is crucial for developing novel strategies for treating diabetes, such as promoting the redifferentiation of β-cells in T2D patients [93]. In addition, *in vitro* culture of human islets leads to EMT and dedifferentiation but increased proliferation [11,94], raising the possibility of exploiting these proliferative properties to produce β-cells for transplantation, as long as this process can be followed by a reversal of EMT and dedifferentiation. Understanding the gene networks essential for β-cell aggregation is also relevant for transplantation therapy, as the establishment of proper cell—cell junctions is crucial for maximal insulin secretion and viability. In summary, the miR-200—Zeb1 axis is involved in regulating many key aspects of β-cell biology, and a better understanding of the mechanisms involved may yield results of basic biological and therapeutic value.

AUTHOR CONTRIBUTIONS

A.C.T. and M.S. designed the study and wrote the manuscript. A.C.T performed most of the experiments and analyzed most of the data. P.N.S. helped with aggregation experiments and performed confocal imaging and analysis. S.G. assisted with cell culture experiments, immunofluorescence staining, and western blotting. L.H. helped with immunofluorescence staining and analysis. All authors read and provided input on the manuscript.

FUNDING

This work was supported in part by the Swiss National Science Foundation (NCCR "RNA Biology and Disease," no. 182880).

CONFLICT OF INTEREST

None declared.

ACKNOWLEDGEMENTS

We would like to thank Hasan Kabakci, Nina Brander, and Regina Kubsch for their excellent technical assistance. We would also like to thank the Functional Genomics Center Zurich (FGCZ) for performing RNA sequencing, with particular thanks to Dr. Susanne Kreutzer for general support and Lennart Opitz for bioinformatics support. We also wish to thank ScopeM for their support in histology services and the staff of the ETH Phenomics Center (EPIC) for their support in animal husbandry.

APPENDIX A. SUPPLEMENTARY DATA

Supplementary data to this article can be found online at https://doi.org/10.1016/j.molmet.2021.101267.

REFERENCES

[1] Saeedi, P., Petersohn, I., Salpea, P., Malanda, B., Karuranga, S., Unwin, N., et al., 2019. Global and regional diabetes prevalence estimates for 2019 and projections for 2030 and 2045: results from the international diabetes federation diabetes atlas. Diabetes Research and Clinical Practice 157(107843):1—10.

[2] Butler, A.E., Janson, J., Bonner-weir, S., Ritzel, R., Rizza, R.A., Butler, P.C., 2003. Humans with type 2 diabetes. Diabetes 52:102—110.

[3] Nolan, C.J., Damm, P., Prentki, M., 2011. Type 2 diabetes across generations: from pathophysiology to prevention and management. The Lancet 378(9786): 169—181.

[4] Bensellam, M., Jonas, J.C., Laybutt, D.R., 2018. Mechanisms of β-cell dedifferentiation in diabetes: recent findings and future research directions. Journal of Endocrinology 236(2):R109—R143.

[5] Weir, G.C., Aguayo-Mazzucato, C., Bonner-Weir, S., 2013. β-cell dedifferentiation in diabetes is important, but what is it. Islets 5(5):233—237.

[6] Roefs, M.M., Carlotti, F., Jones, K., Wills, H., Hamilton, A., Verschoor, M., et al., 2017. Increased vimentin in human α- and β-cells in type 2 diabetes. Journal of Endocrinology 233(3):217—227.

[7] Jesus, D.S. De., Mak, T.C.S., Wang, Y., Ohlen, Y. Von., Bai, Y., Chabosseau, P., et al., 2021. Dysregulation of a Pdx1/Ovol2/Zeb2 axis in dedifferentiated β-cells triggers the induction of genes associated with epithelial-mesenchymal transition in diabetes. Molecular Metabolism 2:101248.

[8] Talchai, C., Xuan, S., Lin, H.V., Sussel, L., Accili, D., 2012. Pancreatic β cell dedifferentiation as a mechanism of diabetic β cell failure. Cell 150(6):1223—1234.

[9] Toren-Haritan, G., Efrat, S., 2015. TGFβ pathway inhibition redifferentiates human pancreatic islet β-cells expanded in vitro. PloS One 10(9):1—17.

[10] Lenz, A., Toren-Haritan, G., Efrat, S., 2014. Redifferentiation of adult human β-cells expanded in vitro by inhibition of the WNT pathway. PloS One 9(11):1—14.

[11] Sintov, E., Nathan, G., Knoller, S., Pasmanik-Chor, M., Russ, H.A., Efrat, S., 2015. Inhibition of ZEB1 expression induces redifferentiation of adult human β cells expanded in vitro. Scientific Reports 5:1—13.

[12] Russ, H.A., Ravassard, P., Kerr-Conte, J., Pattou, F., Efrat, S., 2009. Epithelial-mesenchymal transition in cells expanded in vitro from lineage-traced adult human pancreatic beta cells. PloS One 4(7):1—8.

[13] Bartel, D.P., 2018. Metazoan MicroRNAs. Cell 173:20—51.

[14] Mendell, J.T., Olson, E.N., 2012. MicroRNAs in stress signaling and human disease. Cell 148(6):1172—1187.

[15] Park, S.-M., Gaur, A.B., Lengyel, E., Peter, M.E., 2008. The miR-200 family determines the epithelial phenotype of cancer cells by targeting the E-cadherin repressors ZEB1 and ZEB2. Genes & Development 22(7):894—907.

[16] Belgardt, B.-F., Ahmed, K., Spranger, M., Latreille, M., Denzler, R., Kondratiuk, N., et al., 2015. The microRNA-200 family regulates pancreatic beta cell survival in type 2 diabetes. Nature Medicine 21(6):619—627.

[17] Filios, S.R., Xu, G., Chen, J., Hong, K., Jing, G., Shalev, A., 2014. MicroRNA-200 is induced by thioredoxin-interacting protein and regulates Zeb1 protein signaling and beta cell. Journal of Biological Chemistry 289(52):36275—36283.

[18] Jin, W., Mulas, F., Gaertner, B., Sui, Y., Wang, J., Matta, I., et al., 2019. A network of microRNAs acts to promote cell cycle exit and differentiation of human pancreatic endocrine cells. IScience 21:681—694.

[19] Senfter, D., Madlener, S., Krupitza, G., Mader, R.M., 2016. The microRNA-200 family: still much to discover. Biomolecular Concepts 7(5—6):311—319.

[20] Lamouille, S., Xu, J., Derynck, R., 2014. Molecular mechanisms of epithelial-mesenchymal transition. Nature Reviews Molecular Cell Biology 15(3):178—196.

[21] Krebs, A.M., Mitschke, J., Losada, M.L., Schmalhofer, O., Boerries, M., Busch, H., et al., 2017. The EMT-activator Zeb1 is a key factor for cell plasticity and promotes metastasis in pancreatic cancer. Nature Cell Biology 19(5):518—529.

[22] Burk, U., Schubert, J., Wellner, U., Schmalhofer, O., Vincan, E., Spaderna, S., et al., 2008. A reciprocal repression between ZEB1 and members of the miR-200 family promotes EMT and invasion in cancer cells. EMBO Reports 9(6):582—589.

[23] Bracken, C.P., Gregory, P.A., Kolesnikoff, N., Bert, A.G., Wang, J., Shannon, M.F., et al., 2008. A double-negative feedback loop between ZEB1-SIP1 and the microRNA-200 family regulates epithelial-mesenchymal transition. Cancer Research 68(19):7846—7854.

[24] Brabletz, S., Brabletz, T., 2010. The ZEB/miR-200 feedback loop – a motor of cellular plasticity in development and cancer? EMBO Reports 11(9):670—677.

[25] Title, A.C., Hong, S.J., Pires, N.D., Hasenöhrl, L., Godbersen, S., Stokar-Regenscheit, N., et al., 2018. Genetic dissection of the miR-200—Zeb1 axis reveals its importance in tumor differentiation and invasion. Nature Communications 9(4671).

[26] Stone, R.C., Pastar, I., Ojeh, N., Chen, V., Liu, S., Garzon, K.I., et al., 2016. Epithelial-mesenchymal transition in tissue repair and fibrosis. Cell and Tissue Research 365(3):495—506.

[27] Vannier, C., Mock, K., Brabletz, T., Driever, W., 2013. Zeb1 regulates E-cadherin and Epcam expression to control cell behavior in early zebrafish development. Journal of Biological Chemistry 288(26):18643—18659.

[28] Takagi, T., Moribe, H., Kondoh, H., Higashi, Y., 1998. δEF1, a zinc finger and homeodomain transcription factor, is required for skeleton patterning in multiple lineages. Development 125:21—31.

[29] Lewis, B.P., Burge, C.B., Bartel, D.P., 2005. Conserved seed pairing, often flanked by adenosines, indicates that thousands of human genes are microRNA targets. Cell 120(1):15—20.

[30] Garcia, D.M., Baek, D., Shin, C., Bell, G.W., Grimson, A., Bartel, D.P., 2011. Weak seed-pairing stability and high target-site abundance decrease the proficiency of lsy-6 and other microRNAs. Nature Structural & Molecular Biology 18(10):1139—1146.

[31] Hornstein, E., Shomron, N., 2006. Canalization of development by microRNAs. Nature Genetics 38(6S):S20—S24.

[32] Stark, A., Brennecke, J., Bushati, N., Russell, R.B., Cohen, S.M., 2005. Animal microRNAs confer robustness to gene expression and have a significant impact on 3′UTR evolution. Cell 123(6):1133—1146.

[33] Zmuda, E.J., Powell, C.A., Hai, T., 2011. A method for murine islet isolation and subcapsular kidney transplantation. Journal of Visualized Experiments 50(e2096):1—11.

[34] Bankhead, P., Loughrey, M.B., Fernández, J.A., Dombrowski, Y., McArt, D.G., Dunne, P.D., et al., 2017. QuPath: open source software for digital pathology image analysis. Scientific Reports 7:1—7.

[35] Bolger, A.M., Lohse, M., Usadel, B., 2014. Trimmomatic: a flexible trimmer for Illumina sequence data. Bioinformatics 30(15):2114—2120.

[36] Bray, N.L., Pimentel, H., Melsted, P., Pachter, L., 2016. Near-optimal probabilistic RNA-seq quantification. Nature Biotechnology 34(5):525—528.

[37] Robinson, M.D., McCarthy, D.J., Smyth, G.K., 2010. edgeR: a Bioconductor package for differential expression analysis of digital gene expression data. Bioinformatics 26(1):139—140.

[38] Balwierz, P.J., Pachkov, M., Arnold, P., Gruber, A.J., Zavolan, M., Van Nimwegen, E., 2014. ISMARA: automated modeling of genomic signals as a democracy of regulatory motifs. Genome Research 24(5):869—884.

[39] Gertz, J., Savic, D., Varley, K.E., Partridge, E.C., Safi, A., Jain, P., et al., 2013. Distinct properties of cell type-specific and shared transcription factor binding sites. Molecular Cell 52(1):1—22.

[40] Postigo, A.A., Dean, D.C., 1999. ZEB represses transcription through interaction with the corepressor CtBP. Proceedings of the National Academy of Sciences of the United States of America 96(12):6683—6688.

[41] Spaderna, S., Schmalhofer, O., Wahlbuhl, M., Dimmler, A., Bauer, K., Sultan, A., et al., 2008. The transcriptional repressor ZEB1 promotes metastasis and loss of cell polarity in cancer. Cancer Research 68(2):537—544.

[42] Wang, H., Unternaehrer, J.J., 2019. Epithelial-mesenchymal transition and cancer stem Cells : at the crossroads of differentiation and dedifferentiation. Developmental Dynamics 248:10—20.

[43] Blum, B., Hrvatin, S., Schuetz, C., Bonal, C., Rezania, A., Melton, D.A., 2012. Functional beta-cell maturation is marked by an increased glucose threshold and by expression of urocortin 3. Nature Biotechnology 30(3):261—264.

[44] Efrat, S., 2019. Beta-cell dedifferentiation in type 2 Diabetes : concise review. Stem Cells 37:1267—1272.

[45] Liu, J.S.E., Hebrok, M., 2017. All mixed up: defining roles for β-cell subtypes in mature islets. Genes & Development 31(3):228—240.

[46] Wang, H., Brun, T., Kataoka, K., Sharma, A.J., Wollheim, C.B., 2007. MAFA controls genes implicated in insulin biosynthesis and secretion. Diabetologia 50(2):348—358.

[47] Gröger, C.J., Grubinger, M., Waldhör, T., Vierlinger, K., Mikulits, W., 2012. Meta-analysis of gene expression signatures defining the epithelial-to-mesenchymal transition during cancer progression. PloS One 7(12):e51136.
[48] Comijn, J., Berx, G., Vermassen, P., Verschueren, K., Van Grunsven, L., Bruyneel, E., et al., 2001. The two-handed E box binding zinc finger protein SIP1 downregulates E-cadherin and induces invasion. Molecular Cell 7(6): 1267–1278.
[49] Carvell, M.J., Marsh, P.J., Persaud, S.J., Peter, M., 2007. E-cadherin interactions regulate β-cell proliferation in islet-like structures. Cellular Physiology and Biochemistry 20:617–626.
[50] Rogers, G.J., Hodgkin, M.N., Squires, P.E., 2007. E-cadherin and cell adhesion: a role in architecture and function in the pancreatic islet. Cellular Physiology and Biochemistry 20(6):987–994.
[51] Hauge-Evans, A.C., Squires, P.E., Persaud, S.J., Jones, P.M., 1999. Pancreatic β-cell-to-β-cell interactions are required for integrated responses to nutrient stimuli: enhanced Ca2+ and insulin secretory responses of MIN6 pseudoislets. Diabetes 48(7):1402–1408.
[52] Dissanayake, W.C., Sorrenson, B., Shepherd, P.R., 2018. The role of adherens junction proteins in the regulation of insulin secretion. Bioscience Reports 38(2):1–9.
[53] Bavamian, S., Klee, P., Britan, A., Populaire, C., Caille, D., Cancela, J., et al., 2007. Islet-cell-to-cell communication as basis for normal insulin secretion. Diabetes, Obesity and Metabolism 9(Suppl. 2):118–132.
[54] Meda, P., 2018. Gap junction proteins are key drivers of endocrine function. Biochimica et Biophysica Acta (BBA) - Biomembranes 1860:124–140.
[55] Liu, M., Weiss, M.A., Arunagiri, A., Yong, J., Rege, N., Sun, J., et al., 2018. Biosynthesis, structure, and folding of the insulin precursor protein. Diabetes, Obesity and Metabolism 20(Suppl 2):28–50.
[56] Yi, Z., Yokota, H., Torii, S., Aoki, T., Hosaka, M., Zhao, S., et al., 2002. The rab27a/granuphilin complex regulates the exocytosis of insulin-containing dense-core granules. Molecular and Cellular Biology 22(6):1858–1867.
[57] Balestrieri, C., Alfarano, G., Milan, M., Tosi, V., Prosperini, E., Nicoli, P., et al., 2018. Co-optation of tandem DNA repeats for the maintenance of mesenchymal identity. Cell 173(5):1150–1164.
[58] Inoue-Yamauchi, A., Oda, H., 2020. EMT-inducing transcription factor ZEB1-associated resistance to the BCL-2/BCL-XL inhibitor is overcome by BIM upregulation in ovarian clear cell carcinoma cells. Biochemical and Biophysical Research Communications 526(3):612–617.
[59] Song, K.A., Niederst, M.J., Lochmann, T.L., Hata, A.N., Kitai, H., Ham, J., et al., 2018. Epithelial-to-mesenchymal transition antagonizes response to targeted therapies in lung cancer by suppressing BIM. Clinical Cancer Research 24(1): 197–208.
[60] Gorasia, D.G., Dudek, N.L., Safavi-Hemami, H., Perez, R.A., Schittenhelm, R.B., Saunders, P.M., et al., 2016. A prominent role of PDIA6 in processing of misfolded proinsulin. Biochimica et Biophysica Acta (BBA) - Proteins & Proteomics 1864(6):715–723.
[61] Yoon, S. Bin., Park, Y.H., Choi, S.A., Yang, H.J., Jeong, P.S., Cha, J.J., et al., 2019. Real-time PCR quantification of spliced X-box binding protein 1 (XBP1) using a universal primer method. PloS One 14(7):1–12.
[62] Melkman-Zehavi, T., Oren, R., Kredo-Russo, S., Shapira, T., Mandelbaum, A.D., Rivkin, N., et al., 2011. MiRNAs control insulin content in pancreatic β-cells via downregulation of transcriptional repressors. The EMBO Journal 30(5):835–845.
[63] Hill, L., Browne, G., Tulchinsky, E., 2013. ZEB/miR-200 feedback loop: at the crossroads of signal transduction in cancer. International Journal of Cancer 132(4):745–754.
[64] Martinez-Sanchez, A., Rutter, G.A., Latreille, M., 2017. MiRNAs in β-cell development, identity, and disease. Frontiers in Genetics 7:1–19.
[65] Nesca, V., Guay, C., Jacovetti, C., Menoud, V., Peyot, M.L., Laybutt, D.R., et al., 2013. Identification of particular groups of microRNAs that positively or negatively impact on beta cell function in obese models of type 2 diabetes. Diabetologia 56(10):2203–2212.
[66] Ferrell, J.E., 2002. Self-perpetuating states in signal transduction: positive feedback, double-negative feedback and bistability. Current Opinion in Cell Biology 14(2):140–148.
[67] Cai, S., Zhou, P., Liu, Z., 2013. Functional characteristics of a double negative feedback loop mediated by microRNAs. Cognitive Neurodynamics 7:417–429.
[68] Johnston, R.J., Chang, S., Etchberger, J.F., Ortiz, C.O., Hobert, O., 2005. MicroRNAs acting in a double-negative feedback loop to control a neuronal cell fate decision. Proceedings of the National Academy of Sciences 102(35): 12449–12454.
[69] Lim, J., Thiery, J.P., 2012. Epithelial-mesenchymal transitions: insights from development. Development 139(19):3471–3486.
[70] Puri, S., Roy, N., Russ, H.A., Leonhardt, L., French, E.K., Roy, R., et al., 2018. Replication confers β cell immaturity. Nature Communications 9(1).
[71] Scharfmann, R., Czernichow, P., Scharfmann, R., Pechberty, S., Hazhouz, Y., Bülow, M. Von., 2014. Development of a conditionally immortalized human pancreatic β cell line. Journal of Clinical Investigation 124(5):2087–2098.
[72] Klochendler, A., Caspi, I., Corem, N., Moran, M., Friedlich, O., Elgavish, S., et al., 2016. The genetic program of pancreatic β-cell replication in vivo. Diabetes 65(7):2081–2093.
[73] Rukstalis, J.M., Habener, J.F., 2007. Snail2, a mediator of epithelial-mesenchymal transitions, expressed in progenitor cells of the developing endocrine pancreas. Gene Expression Patterns 7(4):471–479.
[74] Cole, L., Anderson, M., Antin, P.B., Limesand, S.W., 2009. One process for pancreatic β-cell coalescence into islets involves an epithelial-mesenchymal transition. Journal of Endocrinology 203(1):19–31.
[75] Dahl, U., Sjødin, A., Semb, H., 1996. Cadherins regulate aggregation of pancreatic β-cells in vivo. Development 122(9):2895–2902.
[76] Wakae-Takada, N., Xuan, S., Watanabe, K., Meda, P., Leibel, R.L., 2013. Molecular basis for the regulation of islet beta cell mass in mice: the role of E-cadherin. Diabetologia 56(4):856–866.
[77] Serrill, J.D., Sander, M., Shih, H.P., 2018. Pancreatic exocrine tissue architecture and integrity are maintained by E-cadherin during postnatal development. Scientific Reports 8(1):1–12.
[78] Blum, B., Roose, A.N., Barrandon, O., Maehr, R., Arvanites, A.C., Davidow, L.S., et al., 2014. Reversal of β cell de-differentiation by a small molecule inhibitor of the TGFβ pathway. ELife 3(e02809):1–17.
[79] Russ, H.A., Efrat, S., 2011. Development of human insulin-producing cells for cell therapy of diabetes. Pediatric Endocrinology Reviews 9(2):590–597.
[80] Santos-Silva, J.C., Carvalho, C.P. de F., de Oliveira, R.B., Boschero, A.C., Collares-Buzato, C.B., 2012. Cell-to-cell contact dependence and junctional protein content are correlated with in vivo maturation of pancreatic beta cells. Canadian Journal of Physiology and Pharmacology 90(7):837–850.
[81] Bosco, D., Rouiller, D.G., Halban, P.A., 2007. Differential expression of E-cadherin at the surface of rat β-cells as a marker of functional heterogeneity. Journal of Endocrinology 194(1):21–29.
[82] Back, S.H., Kaufman, R.J., 2012. Endoplasmic reticulum stress and type 2 diabetes. Annual Review of Biochemistry 81:767–793.
[83] Papa, F.R., 2012. Endoplasmic reticulum stress, pancreatic β-cell degeneration, and diabetes. Cold Spring Harbor Perspectives in Medicine 2(9):1–17.
[84] Mezza, T., Ferraro, P.M., Sun, V.A., Moffa, S., Cefalo, C.M.A., Quero, G., et al., 2018. Increased β-cell workload modulates proinsulin-to-insulin ratio in humans. Diabetes 67(11):2389–2396.
[85] Szabat, M., Page, M.M., Panzhinskiy, E., Skovsø, S., Mojibian, M., Fernandez-Tajes, J., et al., 2016. Reduced insulin production relieves endoplasmic reticulum stress and induces β cell proliferation. Cell Metabolism 23(1):179–193.

[86] Oyadomari, S., Koizumi, A., Takeda, K., Gotoh, T., Akira, S., Araki, E., et al., 2002. Targeted disruption of the Chop gene delays endoplasmic reticulum stress-mediated diabetes. Journal of Clinical Investigation 109(4):525–532.

[87] Rabhi, N., Salas, E., Froguel, P., Annicotte, J.S., 2014. Role of the unfolded protein response in β cell compensation and failure during diabetes. Journal of Diabetes Research, 1–11.

[88] Scheuner, D., Kaufman, R.J., 2008. The unfolded protein response: a pathway that links insulin demand with β-cell failure and diabetes. Endocrine Reviews 29(3):317–333.

[89] Sun, J., Cui, J., He, Q., Chen, Z., Arvan, P., Liu, M., 2015. Proinsulin misfolding and endoplasmic reticulum stress during the development and progression of diabetes. Molecular Aspects of Medicine 42:105–118.

[90] Cnop, M., Toivonen, S., Igoillo-Esteve, M., Salpea, P., 2017. Endoplasmic reticulum stress and eIF2α phosphorylation: the Achilles heel of pancreatic β cells. Molecular Metabolism 6(9):1024–1039.

[91] de Jesus, D.S., Mak, T.C.S., Wang, Y.F., von Ohlen, Y., Bai, Y., Kane, E., et al., 2021. Dysregulation of the Pdx1/Ovol2/Zeb2 axis in dedifferentiated β-cells triggers the induction of genes associated with epithelial-mesenchymal transition in diabetes. Molecular Metabolism. https://doi.org/10.1016/j.molmet.2021.101248.

[92] Zhu, Y., Sun, Y., Zhou, Y., Zhang, Y., Zhang, T., Li, Y., et al., 2019. MicroRNA-24 promotes pancreatic beta cells toward dedifferentiation to avoid endoplasmic reticulum stress-induced apoptosis. Journal of Molecular Cell Biology 11(9):747–760.

[93] Efrat, S., 2016. Mechanisms of adult human β-cell in vitro dedifferentiation and redifferentiation. Diabetes, Obesity and Metabolism 18:97–101.

[94] Russ, H.A., Bar, Y., Ravassard, P., Efrat, S., 2008. In vitro proliferation of cells derived from adult human β-cells revealed by cell-lineage tracing. Diabetes 57:1575–1583.

